Published in final edited form as:
Virology. 2009 December 20; 395(2): 210–222. doi:10.1016/j.virol.2009.09.023.

A new mouse-adapted strain of SARS-CoV as a lethal model for evaluating antiviral agents in vitro and in vivo

Craig W. Day[a], **Ralph Baric**[b], **Sui Xiong Cai**[d], **Matt Frieman**[c], **Yohichi Kumaki**[a], **John D. Morrey**[a], **Donald F. Smee**[a], and **Dale L. Barnard**[a]

[a] Institute for Antiviral Research, Utah State University, UMC 5600, Logan, Utah, 84322-5600, USA

[b] Department of Microbiology and Immunology, University of North Carolina, Chapel Hill, North Carolina, USA

[c] University of North Carolina, 3105 Hooker Research Center, Chapel Hill, NC 27713, USA

[d] Epicept Corporation, 6650 Nancy Ridge Drive, San Diego, California 92121, USA

Abstract

Severe acute respiratory syndrome (SARS) is a highly lethal emerging disease caused by coronavirus SARS-CoV. New lethal animal models for SARS were needed to facilitate antiviral research. We adapted and characterized a new strain of SARS-CoV (strain v2163) that was highly lethal in 5–6 week old BALB/c mice. It had nine mutations affecting 10 amino acid residues. Strain v2163 increased IL-1α, IL-6, MIP-1α, MCP-1, and RANTES in mice, and high IL-6 expression correlated with mortality. The infection largely mimicked human disease, but lung pathology lacked hyaline membrane formation. In vitro efficacy against v2163 was shown with known inhihibitors of SARS-CoV replication. In v2163-infected mice, Ampligen™ was fully protective, stinging nettle lectin (UDA) was partially protective, ribavirin was disputable and possibly exacerbated disease, and EP128533 was inactive. Ribavirin, UDA and Ampligen™ decreased IL-6 expression. Strain v2163 provided a valuable model for anti-SARS research.

Keywords

SARS-CoV; lethal; IL-6; ribavirin; Ampligen™; UDA; protease inhibitor; cytokine; chemokine; mouse

Introduction

Severe acute respiratory syndrome (SARS) emerged in 2002 in the Guandong province of southern China as a new infectious respiratory disease characterized by influenza-like symptoms and signs, but with a very high mortality rate (Ksiazek et al., 2003; Peiris et al., 2003b). A novel coronavirus termed SARS-CoV was identified as the etiological agent (Drosten et al., 2003a; Drosten et al., 2003b). The World Health Organization (WHO) reported 8,098 SARS cases from November 2002 to July 2003, and approximately 10% of the patients died (http://who.int/csr/sars/country/table2003_09_23/en/). Subsequent outbreaks including

Correspondence to: Dale L. Barnard.

two laboratory events occurred, but they were rapidly contained. These outbreaks demonstrated the need for strategies to treat sporadic cases of SARS disease, including economical lethal rodent models that would simulate human SARS disease.

Studies on the molecular evolution of SARS-CoV suggested that the virus emerged from non-human sources (Guan et al., 2003), although the natural reservoir of the virus has not been positively identified. A current hypothesis is that the horseshoe bat is the main natural reservoir of SARS-CoV-like viruses (Hon et al., 2008; Li et al., 2005b). A number of SARS-CoV-like viruses have been isolated from bats, although the full lineage for the ancestors of SARS-CoV remains uncharacterized (Hon et al., 2008). Virus transmission to humans may have occurred when civet cats, infected by bats, were traded on Chinese wet markets (Guan et al., 2003).

Severe SARS-CoV infections in humans are characterized by diffuse alveolar damage and sparse inflammatory infiltrates (Chen and Subbarao, 2007; Franks et al., 2003; Nicholls et al., 2003). Hyaline membrane formation is a hallmark of SARS-CoV lung damage in humans (Hsiao et al., 2005). In addition to the hyaline membrane formation in severe SARS cases, findings could include serous, fibrinous and hemorrhagic inflammation in pulmonary alveoli with capillary engorgement, including micro-thrombosis in some of these capillaries (Lang et al., 2003). Pulmonary alveoli are thickened with interstitial mononuclear inflammatory infiltrates. Desquamation of pneumocytes can be detected along with fibrinoid materials, and erythrocytes in alveolar spaces (Lang et al., 2003). Cell types in the respiratory tract in which SARS-CoV antigen has been detected include the following: alveolar epithelial cells (primarily type II pneumocytes), bronchial epithelial cells, and alveolar macrophages (Ding et al., 2004; Ye et al., 2007). These cell types all have the angiotensin-converting enzyme 2 (ACE2), which has been identified as one of the receptors to which SARS-CoV binds in order to be taken up into host cells (Li et al., 2005a; 2003).

A number of animal species have been proposed to model SARS infections in human, including macaques (Fouchier et al., 2003), marmosets (Greenough et al., 2005), mice (Glass et al., 2004; Roberts et al., 2005), golden Syrian hamsters (Roberts, 2006), rats (Nagata et al., 2007), cats (Martina et al., 2003; van den Brand et al., 2008), and ferrets (Chu et al., 2008; Martina et al., 2003; Subbarao and Roberts, 2006; van den Brand et al., 2008). The utility of various animal models has been extensively reviewed by Roberts and Subbarao (2006). Briefly, the non-primate models do not exactly model the lung pathology found in humans. For example, hyaline membrane formation is not seen at all or rarely detected. In the rodent models, fever is also not detected. Nevertheless rodent models may be the most utile of the models because of low expense, ease of handling, defined genetics, and the possibility of doing large-scale statistically significant studies. Because of these advantages, a lethal rodent model would be extremely valuable in antiviral drug testing where the amounts of experimental compound available for evaluation in animals are often limited.

Since early in the SARS outbreak, there has been a concerted effort by many laboratories to evaluate vaccines (Du et al., 2009) or to develop clinically approved drugs for efficacy against SARS-CoV to rapidly provide a treatment for SARS infections in humans (Tong, 2009a; Tong, 2009b). To date, there is no approved agent for treating SAR-CoV and no agent has reached human clinical trials (Wong and Yuen, 2008). This is due to lack of animal model testing among other reasons. Ribavirin had been used to treat SARS infections in 2003 and 2004, but its efficacy is questionable and it may exacerbate disease in mice (Barnard et al., 2006b) and humans (Stockman, Bellamy, and Garner, 2006). Wu and others have recently reviewed the state of drug discovery for SARS-CoV antiviral agents (Pyrc, Berkhout, and van der Hoek, 2007; Stockman, Bellamy, and Garner, 2006; Tong, 2009b; Wu et al., 2006; Yeung and Meanwell, 2007). In the current study, we report on the pathogenesis and genetic changes of a SARS-CoV strain, called v2163, which was adapted from SARS-CoV Urbani by 25 serial

passages to cause a lethal pulmonary syndrome in 5–6 week old mice. Using multiple drugs with purported antiviral activity, the utility of the new strain as a model virus for evaluating drugs in cell culture and in mice is shown.

RESULTS

Morbidity and virus titers in mice

The Urbani strain of SARS-CoV, which is not lethal to BALB/c mice, was serially passaged 25 times in BALB/c mice at 3 day intervals and resulted in a highly lethal strain we designated as v2163. The v2163 virus caused severe signs of illness in 5–6 week old BALB/c mice including ruffled fur and lethargy within 3–4 days and death by day 6. Another lethal mouse-adapted strain designated as MA15 (Roberts et al., 2007) was tested in parallel for comparison. Both mouse-adapted strains caused substantial weight loss and produced high virus titers in the lungs of infected mice (Table 1). In contrast, SARS-CoV strain Urbani-infected mice had no significant weight loss compared with uninfected controls, although they had moderate virus titers in the lungs three days post virus exposure as shown previously by Barnard et al. (2006a; 2006b). Lung virus titers at 3 days post virus inoculation (d.p.i.) were higher in v2163-infected mice than in MA15-infected mice. Lung titers did not appear dependent on the level of virus inoculum, but did differ depending on the virus strain. The v2163 virus and MA15 virus persisted in the lungs for 6 days, while Urbani strain was below detection limit by day 6.

Mortality and recovery in mice

Infection with v2163 resulted in 100% of the 5–6 week old mice losing 20% of their initial weight, and 70% to 100% of mice dying depending on the infectious dose (Table 1). Nearly all MA15-infected mice lost more than 20% of their initial weight when infected with $10^{4.5}$ or $10^{5.5}$ $CCID_{50}$ (Table 1), confirming results observed in 6–8 week old mice by Roberts et al. (2007). However, the v2163 strain killed more mice than strain MA15 regardless of the inoculum used (Table 1). The v2163 virus was lethal at concentrations as low as $10^{3.5}$ $CCID_{50}$ per mouse. In a replicate experiment, results were similar to those in Table 1, except 6 of 10 mice receiving $10^{4.5}$ $CCID_{50}$ of MA15 died (Table 2). However, the MA15-infected mice that died had a mean day of death (MDD) of 13.5 ± 6.9 days, compared with 5.9 ± 1.4 MDD for the corresponding v2163-infected group (Table 2). Overall, death of 6-week old mice infected with v2163 was significantly greater ($P < 0.001$) than MA15-infected mice (Figure 1). Recovery from severe illness was more likely for MA15-infected mice than for v2163-infected mice, and v2163 was lethal at a lower infectious dose. The average LD_{50} for v2163 was $10^{3.3\pm0.3}$ $CCID_{50}$ per mouse. These data were unique because, by special provision, animals were not euthanized during severe illness but allowed to die or recover spontaneously.

Age variability

The animal experiment was repeated comparing 5–6 week old mice with 10–11 week old mice (Table 2). The older mice infected with MA15 lost more weight by 4 d.p.i. than corresponding v2163-infected mice, and their MDD was 2–3 days later than v2163-infected mice. Mortality in 10–11 week mice was high for both mouse-adapted virus strains using $10^{5.5}$ and $10^{4.5}$ $CCID_{50}$ inocula. However, only 10% of the MA15-infected mice receiving the $10^{3.5}$ inoculum died, while 100% of the corresponding v2163-infected mice died. No mice died from Urbani infection. Interestingly, in one separate age experiment, only 20% (2/10) of mice 3–4 weeks old died from a $10^{4.0–4.5}$ $CCID_{50}$ v2163 infection, while 100% of 7–8 week old mice died (data not shown). This supported the notion that SARS-CoV was more lethal in older hosts.

Genome sequence

The v2163 virus had 9 mutations, one of which affected two reading frames, resulting in changes to 10 amino acid residues compared with the wild type Urbani. Four mutations occurred in the spike protein (S) region (Figure 2). A putative G-A mutation was observed in base pair 22722 with some replicates, but it was not found in RNA from infected mouse lungs. The mutations were compared to the MA15 lethal strain (Roberts et al., 2007), revealing interesting similarities and differences in the mutation spectra associated with mouse adaptation in young Balb/c mice (Figure 2). In the structural genes, the Y436H mutation in the v2163 spike region was conserved in strain MA15, and the M-mutation was in a similar location on both lethal strains (S6L for v2163, E11K in MA15). In the replicase genes, the nsp9 mutation (E4185D) was located near an nsp9 mutation (T4184A) found in strain MA15, and both lethal strains had an nsp13 mutation.

Cytokines and chemokines

The mouse-adapted strains of SARS-CoV elicited expression of cytokines IL-1α and IL-6, and chemokines MIP-1α, MCP-1, and RANTES in the lungs of mice 3 days after infection as measured with the multiplex ELISA assay (Figure 3). Levels of IL-1β, IL-2, IL-3, IL-4, IL-5, IL-9, IL-10, TNF-α, and GM-CSF were below the minimum detection level for all test groups (≤38 pg/mL of lung homogenate). Low levels of INF-γ were observed with both mouse-adapted strains but not detected with the Urbani strain. Two out of ten v2163-inoculated mice showed low cytokine response, and were excluded from cytokine analysis because they also had little or no virus detected in their lungs. The MA15 virus stimulated significantly more MIP-1α, and RANTES compared with Urbani ($P < 0.05$), and the v2163 virus caused significantly greater MCP-1 response than Urbani ($P < 0.01$). A significantly higher IL-6 response compared with the wild type Urbani strain was observed from both v2163 and MA15 mouse-adapted strains ($P < 0.001$, $P < 0.05$ respectively). The v2163-infected mice expressed 6-fold more IL-6 than the MA15-infected mice. At the infection level used in this experiment, 100% of v2163-infected mice died and no MA15-infected mice died, showing a correlation between IL-6 concentrations in the lungs and mortality.

Histopathology

Three lung samples for each virus or control were evaluated for pathological changes 3 days after inoculation by a board certified veterinary pathologist (Figure 4). Lungs of mice inoculated with the Urbani strain of SARS-CoV showed no significant changes, and sham-infected controls showed no marked changes except some scattered dense granulomas in one of three lungs. All three MA15-infected lungs showed small numbers of foamy macrophages and small numbers of neutrophils. Alveolar septae were seen in two of the three MA15-infected lungs. One MA15-infected lung had rare individual bronchiolar lining cells that were swollen and hypereosinophilic and degenerate. Pathological changes were observed in two of the three v2163-infected lungs; one had moderate numbers of neutrophils, edema fluid surrounding several large vessels, and rare granulomas containing refractile central fragments of foreign material replacing groups of alveoli. Another v2163-infected lung showed small numbers of alveolar macrophages throughout airspaces. In general, lungs infected with MA15 or v2163 showed acute to subacute alveolitis with some perivascular edema in some sections (Figure 4). Differences between the two mouse-adapted strains were minimal. Hyaline membrane formation, as occurs in human SARS patients (Roberts et al., 2005), was not observed.

In vivo efficacy of drugs against v2163 infection

To demonstrate the utility of the lethal mouse model for antiviral drug testing, we evaluated the known antiviral agents ribavirin, an antiviral nucleoside analog (Sidwell et al., 1972), and Ampligen™(poly I:poly $C_{12}U$), a synthetic dsRNA polymer that induces interferon production

(Barnard et al., 2006a; Carter et al., 1972; Gowen et al., 2007). We also evaluated the novel drugs EP128533, a dipeptidyl glutaminyl fluoromethylketone protease inhibitor (Zhang et al., 2006), and UDA, a lectin that impedes viral fusion and egress (Keyaerts et al., 2007). Ampligen™ (10 mg/kg/d) afforded mice complete protection against death, reduced virus titers in the lungs, and significantly reduced lung scores and weight loss (Table 3). UDA treatment of 5 mg/kg/day resulted in 50% protection from death up to 10 days after infection (Table 3), but no reduction in lung virus titer. A replicate 21-day study showed 40% protection and no measurable toxicity with 15 mg/kg/d of UDA (data not shown). Protease EP128533 was inactive in BALB/c mice.

Ribavirin treatment of 75 mg/kg/d did not significantly protect mice from death (Table 3). Virus lung titers from mice treated with ribavirin were no different than those detected from control mice on 3 d.p.i., but at 6 d.p.i. the titers in ribavirin- treated mice were higher than those detected in the control group, suggesting that ribavirin prolonged lung infection, although this difference was not statistically significant (Table 3). Gross pathology (lung scores) at day 6 revealed substantial lung discoloration in ribavirin-treated mice. The MDD in mice treated with ribavirin was reduced (Table 3), but the survivor curve was statistically similar to that of PSS controls (Figure 4). In the second experiment, virus titers were lower than controls in ribavirin-treated mice on day 6 (Table 4), but 50% of that group also died by 6 d.p.i. (data not shown).

The IL-6 concentration in the lungs on 3 d.p.i., was significantly lower ($P < 0.05$) in mice receiving Ampligen™ or ribavirin treatment, and slightly lower with UDA compared with controls (Table 4). EP128533-treated mice showed no difference in IL-6 compared with controls. The uninfected control group had IL-6 levels of 2200 ± 670 pg/mL, which could be a result of stress induced by handling mice during daily weights and twice daily treatments. Therefore, 2200 pg/mL was considered the baseline IL-6 concentration in this study.

Histopathology of mice with varied antiviral treatments showed neutrophil infiltration and degenerate cells (Table 4). Lesions observed by a board certified pathologist were summarized in tabular form, and all lesions observed were included. Lungs in mice treated with a protease inhibitor, EP128533, and cremaphor solvent control appeared to have less overall lesions on 3 d.p.i. than lungs of mice in other treatment groups. Ribavirin-treated lungs had fewer overall lesions than those of other groups on 6 d.p.i. Macrophage infiltration, lymphocyte infiltration, and edema were not detected in infected lungs in this experiment, and no hyaline membrane formation was observed. Histological changes were similar between Ampligen™ treated groups and untreated control groups.

In vitro efficacy testing with strain v2163

The v2163 strain was tested in vitro for sensitivity to multiple antiviral compounds. Compounds were chosen based on their mode of action or purported activity in previous literature. Vero-76 cells were treated with multiple concentrations of each compound then infected with virus, and the 50% effective concentration (EC_{50}), the 50% cytotoxic concentration (IC_{50}), and the selective index (SI) for each compound were calculated (Table 5). Compounds with a high selective index were considered active. The antiviral activity of drugs against v2163 was similar to that of the same compounds against the Urbani strain ($P > 0.05$). Infergen™, a consensus interferon-α (Kumaki et al., 2008), was shown to be highly active, with a 90% effective concentration of <0.65 μg/mL against both strains and SI values >490. Ribavirin, promazine, an antipsychotic drug (Barnard et al., 2008), and calpain inhibitor VI (Barnard et al., 2004) showed no appreciable activity above their cytotoxic concentration (Table 5). EP128533 (Zhang et al., 2006) and UDA were moderately active. Calpain inhibitor IV (Barnard et al., 2004) was slightly active against both SARS-CoV v2163 and Urbani strains, with a 90% effective concentration of 12 and 6.4 μg/mL and SI values of 3.9 and 8.1 respectively. The

v2163 strain appeared less sensitive to calpain inhibitor IV and EP128533 than strain Urbani, although the differences were not statistically significant.

Discussion

We have developed a new mouse-adapted strain called v2163 that causes increased morbidity and mortality in BALB/c mice, which the parent Urbani strain does not do. Strain v2163 was derived from the non-pathogenic Urbani strain of SARS-CoV by serial passage in BALB/c mice. Mice infected with the v2163 strain were less likely to survive SARS-CoV infection than Urbani-infected or MA15-infected mice. The MA15 strain appeared less lethal in the current study than shown by Roberts et al. (2007). However, in the study previously reported, death was based on 20% weight loss. When 20% weight loss was equated to mortality in the current work, the results for MA15 were closely similar to previous reports (Table 1). Further, the prior finding that an inoculum of $10^{3.9}$ $CCID_{50}$ of MA15 per mouse was sublethal (Roberts, et al., 2007) was confirmed in the current work. The reduced lethality of strain MA15 in the current experiments may also be attributed to the use of 5–6 week old mice rather than 6–8 week old mice. In the current study, 5–6 week old mice were much less susceptible to MA15 than were 10–11 week old mice (Table 2). SARS-CoV is known to be more fatal in aged patients than in younger patients (Chen and Subbarao, 2007). Age-related susceptibility to SARS-CoV in mice has been shown previously with 4 week versus 6 month old mice (Nagata et al., 2008), with 12–14 month old mice (Roberts et al., 2005), and between 10 week old and 1 year old mice (Rockx et al., 2007). The lethality of the v2163 virus in younger mice is an advantage for its use as a convenient model for evaluation of potential antiviral treatments.

The v2163 genome contained nine mutations compared with the parent Urbani strain, and these resulted in 10 amino acid residue changes since bp 26133 affects two reading frames. Although the v2163 strain was developed independently, its genome shared mutations with the previously created mouse adapted MA15 strain (Figure 2). The spike mutation Y436H was common to both lethal strains, and is within the receptor-binding motif (Roberts et al., 2007). The Y436H mutation has been shown to enhance infectivity of recombinant viruses in mice (Becker et al., 2008), presumably by providing a more favorable interaction with the mACE2 receptor for docking and entry. The v2163 strain had three mutations in the S (spike) region that were not present in MA15, suggesting that the increased virulence observed with v2163 potentially may be due to binding properties. Moreover, Y442F is a contact interface residue site that engages the ACE2 receptor, and passage of civet strain SZ16 K479N in human airway epithelial cells selected for a similar change at this position, shown to enhance SZ16 S interaction with the hACE2 receptor (Sheahan et al., 2008). Further, in separate work, a Y442L mutation was seen on a third mouse-adapted strain (MA20) in the same amino acid residue as the Y442F mutation of v2163 (Frieman, et al. publication in preparation). Interestingly, the T1181L and N1169D alterations are in the heptad repeat elements in S2 where they could promote fusion and entry or host range expansion (McRoy and Baric, 2008).

Mutations outside of the spike region also appeared to be important. The mutation in the M glycoprotein gene (S6L) is near the MA15 E11K mutation that has been associated with increased production of virus particles from infected cells, presumably by promoting more efficient assembly and release, although the exact mechanism is unknown (Pacciarini et al., 2008). The nsp9 E4185D mutation is located near the nsp9 T4184A mutation of MA15, and likely confers a similar phenotypic difference, presumably increasing virulence. Both lethal strains had an nsp13 mutation, although it is not known if they confer similar changes to the protein structure. The fact that independent selections resulted in similar mutation profiles in target genes supports their role in increased replication and/or pathogenesis. Elucidation of the effects of these specific mutations may be key to understanding the genotypic variations that lead to more lethal phenotypes of SARS-CoV and coronaviruses in general. Such knowledge

could allow rapid synthesis of chimeric viruses for use in evaluating and developing effective antiviral treatments.

Multiple cytokines and chemokines expressed in the lungs of BALB/c mice 3 d.p.i. infected with mouse-adapted SARS-CoV were significantly higher than those found in lungs of mice infected with the Urbani strain of SARS-CoV (Figure 3). IL-6 and MCP-1 were more strongly expressed in v2163-infected mice than in MA15-infected mice. IL-6 and MCP-1 have been observed in human SARS patients (Chen and Subbarao, 2007), and one human study determined that IL-6, IL-8 and MCP-1 indicated a high risk of death (Jiang et al., 2005). Therefore, MCP-1 and IL-6, are likely good early indicators of disease outcome in mice. In contrast, cytokines MIP-1α and RANTES were more elevated in MA15-infected groups than v2163-infected groups. Since MA15-infected mice had lower mortality than v2163-infected mice, MIP-1α and RANTES may not be good indicators of disease outcome. When comparing the mouse cytokine profile to that detected in human SARS patients, the majority of human studies showed the same profile as seen in mice for IL-2, IL-4, IL-6, IL-10, IFN-γ, TNF-α, IP-10 and MCP-1 (Cameron et al., 2008;Chen and Subbarao, 2007;Hsueh et al., 2004;Zhu, 2004)(Table 6). In contrast, IL-1β was not elevated in mouse lungs or in human lungs, but 3 of 5 serum studies reviewed showed elevated IL-1β in human patients. RANTES was elevated in mouse lungs but not in the human sera. However, uninfected controls had elevated RANTES levels in mice as well, so the response was not considered important. IFN-γ was detected in lethally infected mouse lungs but not in human lungs. Nevertheless, the IFN-γ findings were considered consistent with human data since the IFN-γ level in mice was low, and IFN-γ has been found in human serum in some studies but not others. The two mouse-adapted SARS-CoV strains in this study both resulted in similar cytokine profiles (Figure 3).

IL-6 levels were of particular interest. The increase in IL-6 corresponded directly with an increase in mortality in the respective experimental groups. Mice infected with the wild-type Urbani strain showed no signs of disease or death, and they had no IL-6 detected in the lungs, while v2163-infected mice expressed high levels of IL-6. In one replicate study, 100% of v2163-infected mice died, and the average IL-6 level for lung homogenates in that group was 2750 pg/mL with only one mouse lower than 2700 pg/mL. The corresponding MA15-infected group in the same study had 100% recovery after severe illness, and those mice had an average IL-6 concentration of only 520 pg/mL with no sample higher than 900 pg/mL. Similarly, one clinical study found that patients with the poorest outcomes also had high levels of IL-6 secreting cells (Jones et al., 2004). In the current work, infected mice receiving PSS, cremaphor and EP128533 groups showed higher IL-6 concentrations than the ribavirin, Ampligen™ and UDA groups (Table 4). The lower IL-6 concentration on 3 d.p.i. coincided with treatments that afforded at least some protection against death in the survival study (Table 3).

The role of IL-6 in SARS-CoV infection merits further investigation. IL-6 is critical in B-cell maturation and acute-phase responses (Kopf et al., 1994), and it is critical in coordination of immune response (Gowen et al., 2006). Conversely, a study reported by Hegde, Pahne, and Smola-Hess (2004) suggests that IL-6 also has immunosuppressive properties. However, high expression of IL-6 may exacerbate disease. In SARS patients, damage to the lung seems to be primarily by viral destruction of alveolar and bronchial epithelial cells and macrophages (Chen and Subbarao, 2007). However, elevated IL-6 levels and concomitant lung damage continued even after peak virus production, which suggests that IL-6 contributes to disease progression (Wang et al., 2004). Furthermore, a SARS patient study showed altered liver function, leucopenia, lymphopenia, thrombocytopenia, and subsequent respiratory distress syndrome, suggesting that there was inflammatory damage resulting from SARS-CoV infection (Peiris et al., 2003a). Studies with other viruses also suggest that excess production of IL-6 may exacerbate disease. For example, a study of herpes simplex virus (HSV) suggested that exuberant production of IL-6 in neonates may explain why sepsis syndrome is more common

with HSV infection in neonates than in adults (Kurt-Jones et al., 2005). A study of phlebovirus infection also proposed that IL-6 contributes to pathogenesis (Gowen et al., 2006). Regardless of the cause-effect relationship, we found that IL-6 is strongly expressed in the lungs during infection with mouse-adapted SARS-CoV virus and may be an effective predictor of disease outcome.

The histopathology of SARS is difficult to distinguish because most lesions observed with SARS can be found with many infections. The main distinguishing histopathological factors in human SARS disease are consolidation, edema, and hyaline membrane formation (Guo et al., 2008). Also, inflammatory infiltrates, usually comprised of mostly macrophages and lymphocytes, are disproportionately low in number with respect to the alveolar damage, and sometimes absent (Chen and Subbarao, 2007; Cheung et al., 2004; Guo et al., 2008). In the current study, lungs infected with mouse-adapted strains of SARS-CoV showed acute to subacute alveolitis with some perivascular edema in some sections. Mice lungs had slight to moderate neutrophil and macrophage infiltration, but lymphocytes were not observed. Erythrocyte infiltration and some fibrinous material were observed with v2163 in some experiments not shown. No hyaline membrane was formed in the mouse lungs. Since lung pathology differed from human disease, and since mice groups that died from infection had similar pathology to that of treated mice that survived infection (Table 5), we submit that histopathology will not be an important marker in this SARS model.

SARS infects multiple tissues in humans, including spleen, intestines, kidneys, liver, adrenal, parathyroid, pituitary, cerebrum, and pancreas and neurons of CNS (Chen and Subbarao, 2007; Guo et al., 2008). With v2163, infectious virus was consistently found in the lung and snout of v2163 inoculated mice on day 3 and day 6 post inoculation, but was only rarely seen in serum. Virus was not recovered from kidney, brain, spleen, intestine, liver, or heart of v2163-infected mice with limits of detection of 2.1 log $CCID_{50}$ for kidney, and 1.1 log $CCID_{50}$ for brain, spleen, and heart, and 4.1 log $CCID_{50}$ for liver and intestine (data not shown). With MA15, Roberts et al. (2007) reported low titers of infectious virus found in lung, brain, spleen and liver of mice infected with MA15.

Ribavirin, Ampligen™, EP128533, and UDA treatments were selected to assess the new v2163 strain of SARS-CoV as a model for in vivo evaluation of potential antiviral drugs. These drugs where chosen to represent a variety of modes of action.

Ribavirin is a known antiviral compound (Sidwell et al., 1972) with multiple modes of action, most of which stem from inhibition of inosine monophosphate dehydrogenase (IMPDH) leading to depressed intracellular GTP levels (Streeter et al., 1973). We had previously found in a mouse virus lung replication model of SARS-CoV that ribavirin extended the time that virus could be detected in the lungs of mice (Barnard et al., 2006b), and this was also observed in one trial of the current study (Table 3). The prolonged high lung titers observed suggested that ribavirin may contribute to the pathogenesis of SARS-CoV by prolonging and/or enhancing viral replication in the lungs, allowing continual stimulation of the inflammatory response, which may contribute to pathogenesis (Perlman and Dandekar, 2005). Also, ribavirin is known to be somewhat toxic, causing hemolytic anemia and other adverse side effects (Wong and Yuen, 2008), so ribavirin would presumably exacerbate disease if there were no concomitant antiviral effect. Interestingly, exacerbation of viral disease by ribavirin has also been shown with West Nile Virus, resulting in increased mortality in hamsters (Morrey et al., 2004) and possibly in human patients (Chowers et al., 2001). In contrast, the second experiment in the current work showed significantly decreased IL-6 concentrations on 3 d.p.i. and somewhat decreased virus titers in ribavirin-treated animals on 6 d.p.i., suggesting some effect of ribavirin in mice (Table 4). The IL-6 reduction with ribavirin was interesting in light of previous reports that ribavirin inhibited IL-6 production in respiratory epithelia cells infected

with RSV virus (Jiang, Kunimoto, and Patel, 1998) and endothelial cells infected with Dengue virus (Huang et al., 2000). However, IL-6 was not reduced by ribavirin in activated T-cells (Hultgren et al., 1998), and ribavirin treatment did not reduce SARS-CoV viral load or IL-6 in human SARS patients (Wang et al., 2005). Ribavirin has not been shown to be effective against SARS in humans. In 2006, systematic review and comprehensive summary of treatments used for SARS patients found that 26 studies with ribavirin were inconclusive and that four showed possible harm (Stockman, Bellamy, and Garner, 2006). However, a 2008 review stated that ribavirin treatment combined with protease inhibitors could be useful clinically, although randomized controlled trials were still needed (Wong and Yuen, 2008). Another study showed synergy with ribavirin in combination with IFN-β in vitro (Morgenstern et al., 2005). Additional research is required to draw more certain conclusions about ribavirin in mice, including age-related studies and drug combination experiments using the lethal v2163 virus as a model.

Ampligen™, poly(I:C$_{(12)}$U), is a synthetic dsRNA polymer that stimulates production of interferon (Carter et al., 1972; Gowen et al., 2007). Ampligen™ has been shown to be effective in vivo against multiple viruses, including Coxsackie virus (Padalko et al., 2004), Venezuelan equine encephalitis (VEE) virus (Julander et al., 2008), punta toro virus (Sidwell et al., 1994), Modoc virus (Leyssen et al., 2003), duck hepatitis B virus (Niu et al., 1993), Banzi virus (Pinto, Morahan, and Brinton, 1988), herpes simplex type 2 (HSV-2) virus (Pinto, Morahan, and Brinton, 1988), and Pichinde virus (Smee et al., 1993). In a virus replication model, Ampligen™ at 10 mg/kg was previously found to afford protection against SARS-CoV replication in the lungs (Barnard et al., 2006a). SARS-CoV is known to be sensitive to type I interferons, IFN-α/β (Cinatl et al., 2003; Stroher et al., 2004). Normally, in the presence of double-stranded RNA or 5′-triphosphorylated ssRNA such as in viral infection, IFNs are synthesized and secreted by infected cells and stimulate expression of potent antiviral proteins (Sadler and Williams, 2008; Samuel, 2001). However, IFN pathways are blocked in cells infected with SARS-CoV (Frieman, Heise, and Baric, 2008), thus making the host more susceptible to infection. We believe that exogenous stimulation of IFN pathways with Ampligen™ overcomes the evasion of virus sensing and signaling pathways. Furthermore, Kuri et al. suggested that “priming” with small amounts of IFN helps the cells themselves restore their normal IFN response to SARS-CoV (2009). In the current study, Ampligen™ appeared not to affect virus replication initially, but led to more rapid decline of virus in the lungs compared with untreated animals by 6 d.p.i. (Table 3). The study showed that Ampligen™ protected against death and gross damage to the lungs in the presence of lethal SARS-CoV.

Stinging nettle lectin (Urtica doica agglutinin, UDA) is an N-acetyl glucosamine-specific lectin that was reported as efficacious against HIV (De Clercq, 2000). More recently, UDA was reported to inhibit coronaviruses in vitro with some selectivity (van der Meer et al., 2007a). Keyaerts et al. (2007) showed that UDA was a potent and selective inhibitor of SARS-CoV strain Frankfurt-1. Plant lectins like UDA probably target viral attachment and fusion, and exocytosis or egress of the virus from the cell (Balzarini, 2007; van der Meer et al., 2007b). The reduction of IL-6 in lungs at 3 d.p.i. along with 50% survival of mice in this study provide evidence to support further investigation of UDA treatment regiments as potential antiviral therapies.

Zhang et al. (2006) reported the design and synthesis of a SARS-CoV protease inhibitor EP128533, 4-(Z-Val-amido)-6-fluoro-5-oxohexanoic acid dimethylamidea, chemical formula $C_{21}H_{30}FN_3O_5$ and molecular weight 423. It was shown to inhibit replication of SARS-CoV strains FFM1 and 6109 in Vero and CaCO2 cells. In the current study, EP128533 was active in cell culture against the Urbani and v2163 strains of SARS-CoV (Table 5), but it was not efficacious in preventing death or reducing the disease signs measured in BALB/c mice (Tables

3 and 4). Since EP128533 is relatively insoluble, the lack of activity is likely because it is not bioavailable in the animal. EP128533 in uninfected mice was not toxic, and replicate trials using DMSO as the solvent yielded similar results as with cremaphor (data not shown). Nevertheless, based on in vitro results, this compound may be a foundation for an effective antiviral protease if a prodrug is developed to make it more soluble and bioavailable.

In vitro sensitivity to antiviral compounds of the v2163 strain was similar to that of strain Urbani ($P > 0.05$) when the two strains were tested in parallel against multiple compounds. In vitro data confirmed recent findings by Barnard et al. (Barnard et al., 2008; Barnard et al., 2006b) that promazine, an antipsychotic drug, and ribavirin, a nucleoside analog, were not effective against SARS-CoV in vitro. Findings with v2163 supported prior findings that Infergen™ was active in vitro against SARS-CoV Urbani (Kumaki et al., 2008). Protease inhibitor EP128533 was active in vitro, as shown previously (Zhang et al., 2006). The current in vitro results showed no marked activity with a calpain inhibitor VI, and slight to moderate activity with calpain inhibitor IV. A previous report showed greater antiviral activity with calpain inhibitor VI than with calpain inhibitor IV (Barnard et al., 2004), and the differences were attributed to greater cell sensitivity to drug toxicity in the previous work, inoculum variation between studies, and stronger virus replication in mammalian cell culture during the current study. UDA was found to be moderately active with antiviral selectivity (SI = 19–22), as with previous work (Keyaerts et al., 2007). Therefore, the v2163 strain was shown to be effective for evaluating antiviral compounds in vitro using microscopic cytopathic effect, neutral red assays, and virus yield reduction tests. Using the v2163 strain in various in vitro assays allowed detection of a highly active compound and various inactive compounds. This will facilitate future analysis of antiviral compounds, since they can be screened in vitro with the v2163 strain and tested in vivo with the same strain.

In conclusion, the new v2163 mouse-adapted strain of SARS-CoV was highly virulent in BALB/c mice 5–6 weeks old, even with infectious doses as low as $10^{3.5}$ $CCID_{50}$ per mouse. Infection with v2163 caused signs of disease, a strong immunological response, and lung pathology. The v2163 infection largely simulated human disease, except that hyaline membrane formation was not detected in the lungs, and infectious virus was not found in tissues outside of the respiratory tract, as is characteristic in human infection (Chen and Subbarao, 2007). Mutations in the virus were consistent with those seen in another mouse-adapted strain, and these may be useful in identifying genotypic markers for lethality. The v2163 strain propagated well in cell culture and was shown to be suitable for in vitro screening of potential antiviral compounds against SARS-CoV. Strain v2163 was used effectively as an in vivo model to evaluate SARS-CoV therapies, showing that Ampligen™ pretreatment was active against lethal SARS-CoV infection, and that UDA may have antiviral effects as well. This new model will facilitate identification of valuable antiviral compounds against SARS-CoV and against future emerging pathogens related to SARS-CoV.

Materials and Methods

Mice, cells, media

Female BALB/c mice were obtained from Charles River Laboratories (Wilmington, MA). They were maintained on Wayne Lab Blox and tap water ad libidum. They were quarantined for >24 h prior to use. Cells used were Vero-76 (ATCC CRL1587), Vero E6 (ATCC CRL1586), and Vero (ATCC CCL81) cells maintained in MEM supplemented with 10% fetal bovine serum (FBS) and no antibiotics. For virus titer tests, MEM with 2% FBS and 50 μg/mL gentamicin was used.

Test compounds

Ribavirin was provided by ICN Pharmaceuticals (Costa Mesa, CA). Calpain inhibitor IV and calpain inhibitor VI were obtained from CalBiochem (San Diego, CA). Infergen™ was interferon alfacon-1 lot 002586 kindly provided by Intermune, Inc. (Brisbane, CA) in 27 μg/mL solution and held frozen until tested. Ampligen™ from Hemispherx Biopharma, Inc. was obtained through the NIAID Antiviral Substances Program. Promazine HCl was obtained from Sigma Chemical Corporation (St. Louis, MO). EP128533 was obtained from Epicept Corporation (San Diego, CA) and through the NIAID Antiviral Substances Program. Stinging nettle lectin (UDA) was obtained from EY Laboratories, Inc. (San Mateo, CA). Compounds were suspended in DMSO or purified water at 20 mM, then diluted in minimal essential medium (MEM) as needed for in vitro assays. Compounds for in vivo assays were diluted in saline, except protease inhibitor EP128533, which was diluted in a cremaphor vehicle (10% cremaphor, 10% ethanol, 80% purified water).

Viruses

MA15 virus—The MA15 strain of SARS-CoV mouse-adapted virus was kindly provided by Dr. Kanta Subbarao, National Institute of Health, NIAID, designated “MA-15 3A-1 P1 in Vero cells 4/25/2005.” For cytokine and lung pathology, MA15 virus was infected into BALB/c mice, then the mouse lung homogenates containing the virus were filtered and subcultured again in Vero (ATCC CCL-81) cell culture for 2 days. Cell culture homogenates were sonicated then frozen at −80°C. For all other in vivo work, the MA15 virus was subcultured in Vero E6 cells in MEM with 10% FBS, 1 mM sodium pyruvate and 0.1 mM non-essential amino acids. After a two day incubation, cell culture homogenates were sonicated, centrifuged to clarify the solution, then aliquotted and held frozen at −80°C. Subcultured stocks were verified by PCR using primers flanking characteristic mutations.

Urbani virus—Severe acute respiratory syndrome coronavirus (SARS-CoV), strain Urbani (200300592), was obtained from the Centers for Disease Control and Prevention (CDC, Atlanta, GA) and routinely passaged in Vero 76 cells.

Mouse-adapted SARS-CoV v2163—Three BALB/c mice were anesthetized with Ketamine/Xylazine mixture (approximately 100 mg/kg + 5 mg/kg respectively) and infected with 50 μL or 100 μL of SARS-CoV Urbani virus solution by nasal inhalation. Three or five days after infection, mice were euthanized, and the lungs were removed and homogenized in 5 mL of MEM + 10% FBS. The homogenate was tested for virus titer by CPE endpoint dilution assay, then re-infected into a subsequent group of mice. These infection steps continued for 25 passages, five passages with the homogenate diluted 1/5, then 20 additional passages without dilution of the lung homogenate between groups. This was determined to be valid because control mice demonstrated no notable effect from inhalation of uninfected lung tissue. One interim passage, P-12, was plaque purified. Passages ceased when increased virus titer in the lungs and signs of illness were observed in the infected animals. Lung homogenate from passge-25 mice was filtered and subcultured in Vero 76 cells, then diluted and plated to isolate single plaques. Plaque purification in Vero76 cells was repeated 3 times. Four isolated plaques were subcultured in Vero-76 cells then compared by infecting into BALB/c mice. The most virulent isolate was selected. Aliquots of the virus stock were incubated in MEM medium for seven days and demonstrated no growth of extraneous bacteria or fungi. RNA was isolated from the virus stock using the RNA-easy kit (Qiagen, Alameda, CA) and tested by qRT-PCR with two primer pairs to verify the presence of SARS-CoV sequences (Accession #AY278741). The presence of SARS-CoV antigen in the virus stock was also demonstrated using the SARS-CoV Ag Detection kit (Wantai Inc., China). The new virus stock was designated “SARS-CoV USU strain v2163” and was used for subsequent studies. It is hereafter referred to as v2163.

Genome sequence

Sequence analysis was then performed at the University of North Carolina. RNA was purified from the cell lysate of Vero-76 cells infected with SARS-CoV V2163 using the RNAeasy kit (Qiagen, Alameda, CA) followed by first-strand cDNA synthesis by reverse transcription using Superscript II (Invitrogen, Carlsbad, CA) as per the manufacturers' protocol. Reverse transcription was performed with an initial incubation of 65 °C for 5 min then cooled on ice followed by a 50-min incubation at 42 °C and a 5-min denaturation at 70 °C. Two microliters of each cDNA reaction were amplified by PCR using Accuprime High Fidelity Taq Polymerase (Invitrogen, Carlsbad, CA). Fifteen pairs of primers were used to generate the overlapping PCR products spaced every 2.5 Kb generating DNA fragments with 500 bp overlap at each end. Amplification products were visualized on agarose gels and purified by use of the QIAquick Gel Extraction Kit (Qiagen, Alameda, CA). PCR products were sequenced in both forward and reverse directions with primers spaced every 500 bp along the genome. Automated sequencing was performed utilizing the BigDye Terminator version 3.1 Cycle Sequencing Kit (Applied Biosystems, Foster City, CA) as per manufacturer's instructions on an ABI Prism 3730 DNA Analyzer (Applied Biosystems). Sequences were assembled and analyzed with Vector NTI and Auto Assembler DNA Sequence Assembly Software (ABI Prism; Applied Biosystems). When a mutation was identified in comparison with the SARS-CoV published sequence (Urbani accession #AY278741), independent RT-PCR reactions were run and subsequent RT-PCR products were sequenced through the region containing the putative mutation to confirm the mutation.

Mouse virulence studies

Mice 5–6 weeks old (14–16 grams) were separated into groups of 10 mice for sacrifice on days 3 and 6 post infection, and 9 or 10 mice for weight and survival data. Mice were anesthetized by 0.1 mL intraperitoneal injection of ketamine (100 mg/kg)/xylazine (5 mg/kg) and then infected intranasally with a 50 μl suspension of the virus. Mice were inoculated with approximately $10^{5.5}$, $10^{4.5}$, and $10^{3.5}$ $CCID_{50}$ of v2163 or MA15. Plaque assays were performed in Vero 76 cells on the actual inocula after infection and showed that the MA15 virus titer was equal or higher than that of the corresponding v2163 titer for both replicate experiments. As a wild type control and for comparison, mice were inoculated with approximately 10^5 $CCID_{50}$ of the Urbani SARS-CoV strain. Groups of 5 and 10 mice were sham infected with MEM as a negative control. The groups of 10 survival mice were weighed individually to the nearest 0.1 gram each day, and observed daily for death. Animals were held until death naturally occurred or up to 21 d.p.i. Three days and 6 d.p.i., 5 survivors in each group were euthanized and the lungs removed. Lungs were then diluted 1:20 in MEM + 10% FBS, homogenized, and held at −80 °C for virus titer testing. Lung homogenates were later thawed and serially diluted in MEM + 2% FBS in triplicate in 96-well plates to obtain $CCID_{50}$ values by the endpoint dilution method described below for virus yield reduction assays. The mean day of death (MDD) was calculated using mice that died and excluding survivors. The study was repeated in 5–6 week old mice and also performed once in 10–11 week old (17–21 gram) mice. Another study was performed as above, with just the $10^{4.5}$ inoculum in BALB/c mice of various ages to determine the age-dependent susceptibility to lethal infection.

Cytokine and chemokine analysis

Groups of 15 mice (14–18 g) were inoculated intranasally with the three virus strains suspended in 50 μL of MEM solution, and controls were mock infected with saline. Inocula ($CCID_{50}$ per mouse) were 4.1 ± 0.3 log $CCID_{50}$ for Urbani, 4.2 ± 0.4 for v2163, and 4.0 ± 0.5 for MA15. On day 3 post virus exposure, five surviving mice were euthanized and the lungs harvested. Remaining mice were held for measurements of weight loss and death. Lung sections were

saved for histopathology in formalin solution. The remaining lung section was diluted 1:20 in MEM solution and homogenized, then held frozen at −80 °C. Samples were then tested for cytokines IL-1α, IL-1β, IL-2, IL-3, IL-4, IL-5, IL-6, IL-9, IL-10, TNF-α, GM-CSF and INF-γ, and for chemokines MIP-1α, MCP-1, and RANTES using the Q-Plex™ mouse cytokine array screen (Quansys Bioscience, Logan, Utah), a quantitative ELISA-based test with multiple distinct capture antibodies absorbed to each well of a 96-well plate in a defined array. Cytokines were quantified by relative luminescence of each spot in the array, and values (pg/mL) calculated using the concurrently-run Quansys Bioscience™ standard curve and the QuansysAnalysys™ software (version 3.4). In one replicate some MCP-1 and RANTES values exceeded the standard curve range and were estimated by extrapolation (Figure 3). Two of ten v2163-inoculated mice had abnormally low cytokines and were excluded as outliers because they had little or no virus detected in the lungs. The cytokine results from all mice from the two experiments were combined for averages, standard deviation, and Kruskal-Wallis analysis of variance followed by Dunn's multiple comparison test compared to Urbani-infected mice.

Histopathology

Groups of animals were infected as described for the cytokine assay above. After three days, lungs from sham controls and mice exposed to 10^4 $CCID_{50}$ Urbani, 10^4 v2163, 10^5 MA15 and were formalin-fixed. Three lungs from each group were sectioned and stained with H&E stain and evaluated by a board certified veterinary pathologist for histopathological changes.

In vivo efficacy of drugs against v2163 infection

Groups of mice (16–19 g) were inoculated with 50 μL containing $10^{4.0}$–$10^{4.4}$ $CCID_{50}$ of v2163 virus by the i.n. route. Groups of mice were administered 100 μL of the following drugs by the intraperitoneal (i.p.) route: ribavirin 32.5 mg/kg twice a day 8 hours apart for 4 days beginning 4 hours prior to exposure to virus; Ampligen™ at 5 mg/kg for 4 treatments 12–16 hours apart beginning 16 hours before virus exposure; and physiological saline solution (PSS) as a placebo using the dosing regimen described for ribavirin. In separate studies, 16–18 g mice were treated with UDA at 5 mg/kg/d using the treatment regiment described above for ribavirin, and 18–20 gram mice were treated with 30 mg/kg/d of EP128533 protease suspended in 10% cremaphor administered b.i.d. as above for 5 days beginning at time of infection. Mice for toxicity controls were treated with PSS or cremaphor diluent using the treatment regimes described above but without virus exposure. Mice were observed daily, and group weights were taken periodically throughout the test period. The average weight loss was calculated on 3 d.p.i., and significance between treatments evaluated by one-way analysis of variance followed by Newman-Keuls multiple comparison test. Compound toxicity in uninfected mice was evaluated in terms of weight change and adverse events, and no drug toxicity was observed in this study.

On days 3 and 6 post infection, three to five surviving mice from each treatment group were sacrificed. The remaining mice were held and observed for death up to day 14 post virus exposure (10 days for UDA). Animals that lost greater than 30% of their initial body weight in this experiment were humanely euthanized and the day of euthanasia was designated as the day of death. Lungs from sacrificed mice were observed for gross pathology and discoloration and assigned a score ranging from 0 (normal appearing lung) to 4 (maximal plum coloration in 100% of lung). Mouse lung samples from each test group were pooled and homogenized in MEM solution and assayed in duplicate for infectious virus using the method described below for virus yield assays using triplicate wells of Vero 76 cells. Titers were compared to controls by analysis of variance on log-transformed values assuming equal variance and normal distribution.

The procedures above were repeated in 15–18 gram mice for IL-6, histopathology, and virus titers in lungs and multiple tissues on 3 and 6 d.p.i. Lung sections were placed in formalin and examined for histopathology as described above. Remaining lung portions were homogenized individually in 2 mL of MEM + 10% FBS and held frozen at −80°. Samples were thawed, mixed, and then tested for IL-6 levels using the eBioScience (San Diego, CA) IL-6 ELISA kit per manufacturer's instructions. Samples size was three per treatment group for histopathology, 4 or 5 for IL-6 and virus titer depending on number of survivors remaining. Values in pg/g of lung were converted to pg/mL corresponding with the 1/20 dilution used in the initial untreated mice (Figure 3). A low outlier in saline day 3 (655 pg/mL) was included in results but excluded from statistical analysis. IL-6 levels in treated groups were compared to untreated controls by ANOVA with Newman-Kuels pairwise comparisons. Individual tissues were harvested with separate sterile instruments to ensure that each tissue was isolated from the lung during necropsy. Tissues were homogenized and titers performed as described for lungs above.

In vitro efficacy testing with strain v2163

The antiviral activity of test compounds was evaluated using the v2163 mouse-adapted virus strain as an in vitro model compared with strain Urbani run concurrently. Antiviral activity was measured by inhibition of virus-induced cytopathic effect (CPE) (Sidwell and Huffman, 1971), neutral red (NR) dye uptake (McManus, 1976), and also by virus yield reduction assays. Vero-76 (ATCC CRL 1587) cells grown in MEM with 10% fetal bovine serum (FBS) were seeded into 96-well plates at a concentration of 2×10^4 cells per well and grown overnight at 37°C with 5% CO_2. Test compounds were dissolved in DMSO or water, then serially diluted in MEM by half-log dilutions in triplicate wells. Test wells were infected with a multiplicity of infection (MOI) of less than 0.007 $CCID_{50}$ per cell, sufficient to cause near complete cytopathic effect (CPE) in three days, which was 1.6 to 2.1 log $CCID_{50}$ per well for Urbani, and 1.0 to 2.4 log $CCID_{50}$ per well for v2163. The test medium was MEM with 2% FBS and 50 μg/mL gentamicin. Toxicity of compounds was assayed in duplicate wells without virus. Plates were incubated as above for three days, then each well read microscopically for CPE. Cells were incubated with 0.011% NR dye for two h at 37 °C. Free dye was removed from the wells, then the uptaken dye was eluted with 50% ethanol in Sorensen citrate buffer for >30 min. Absorbance was then measured as described by Finter (1969), with an Opsys MR microplate reader (Dynex, Chantilly, VA) at 540 and 405 nm. Absorbance values and visual CPE were expressed as percentages of cell controls and untreated virus controls, adjusted for toxicity. The 50% effective concentration (EC_{50}) and 50% inhibitory concentration (cytotoxic, IC_{50}) values were calculated by regression analysis.

Virus yield reduction assays were performed using the cell culture 50% infectious dose ($CCID_{50}$) assay essentially as described previously (Smee et al., 1992). Briefly, supernatants from each well were serially diluted in triplicate wells of 96-well plates containing Vero-76 cells. Plates were incubated six days and then checked for virus-induced CPE. Quantitation of virus yield titers was by the end point method of Reed and Muench (1938). The EC_{90} value was calculated using linear regression to estimate the concentration necessary to inhibit virus yield by 90% or a one $\log_{10}$ decrease in virus titer. Results of at least three assays were averaged and activity with the two virus strains was compared by student's t test.

Statistical analyses

Statistical analyses were performed using PRISM™ 5.01 for Windows, PRISM™ 4.0c for MAC (GraphPad Software, Inc., La Jolla, CA), and Microsoft Excel 11.5. Comparisons not otherwise detailed were performed by the student's two-tailed t-test assuming normal distribution and equal variance, and more sophisticated analyses performed if differences were observed. The Kolmogorov-Smirnov test (KS test) for normal distribution and Bartlett's test for equal variance were performed as applicable. MDD, cytokine values, and gross lung score

data were analyzed by Mann-Whitney pairwise comparisons or the Kruskal-Wallis test followed by Dunn's multiple comparison test as applicable. Surviving animals were not included in MDD calculations. Raw survival numbers were compared by the Fisher exact test. Survivor curve analysis (as in Figure 1) was done using the Kaplan-Meier method and a log rank test. When that analysis revealed significant differences among the treatment groups, pairwise comparisons of survivor curves were analyzed by the Gehan-Breslow-Wilcoxon test, and the relative significance was adjusted to a Bonferroni-corrected significance threshold for the number of treatment comparisons made. Differences in percent weight loss were tested by one-way ANOVA with Newman-Keuls multiple comparison test, assuming equal variance and normal distribution. For lung titer data, we performed a KS test for normality, then used non-parametric Kruskal-Wallis test with Dunn's multiple comparison test for groups that were not normally distributed, and a one-way ANOVA with Newman-Keuls multiple comparison test for groups that were normally distributed. LD_{50} was calculated using Probit analysis (StatPlus: MAC 2009).

Ethics and biosafety

This study was conducted in accordance with the approval of the Institutional Animal Care and Use Committee of Utah State University dated 21 September, 2004. The work was done in the AAALAC-accredited Laboratory Animal Research Center of Utah State University. The U. S. Government (National Institutes of Health) approval was renewed 27 February 2002 (Assurance no. A3801-01) in accordance with the National Institutes of Health Guide for the Care and Use of Laboratory Animals (Revision; 1996). By special provision, animals for lethality comparisons were allowed to survive without compassionate euthanasia until death naturally occurred in order to distinguish weight loss and mortality. All experiments involving infectious SARS-CoV were carried out in BSL-3+ laboratories, and all personnel wore complete body protective coverings and HEPA-filtered powered air purifying respirators.

Acknowledgments

We thank Dixon Grant, Justin Madsen, John Woolcott, Miles Wandersee, and Kevin Bailey for technical assistance; Justin Hoopes and Brian Gowen for professional consultation; Larry Blatt and Scott Seiwert for providing Interferon™. This study was supported by contracts NO1-A1-30048 (Institute for Antiviral Research, IAR), NO1-AI-15435 (IAR), and 5P01AI059443 (Univ. No. Carolina) from Virology Branch, National Institute of Allergic and Infectious Diseases, NIAID.

BIBLIOGRAPHY

Balzarini J. Carbohydrate-binding agents: a potential future cornerstone for the chemotherapy of enveloped viruses? Antivir Chem Chemother 2007;18(1):1–11. [PubMed: 17354647]

Barnard DL, Day CW, Bailey K, Heiner M, Montgomery R, Lauridsen L, Chan PK, Sidwell RW. Evaluation of immunomodulators, interferons and known in vitro SARS-coV inhibitors for inhibition of SARS-coV replication in BALB/c mice. Antivir Chem Chemother 2006a;17(5):275–84. [PubMed: 17176632]

Barnard DL, Day CW, Bailey K, Heiner M, Montgomery R, Lauridsen L, Jung KH, Li JK, Chan PK, Sidwell RW. Is the anti-psychotic, 10-(3-(dimethylamino)propyl)phenothiazine (promazine), a potential drug with which to treat SARS infections? Lack of efficacy of promazine on SARS-CoV replication in a mouse model. Antiviral Res 2008;79(2):105–13. [PubMed: 18423639]

Barnard DL, Day CW, Bailey K, Heiner M, Montgomery R, Lauridsen L, Winslow S, Hoopes J, Li JK, Lee J, Carson DA, Cottam HB, Sidwell RW. Enhancement of the infectivity of SARS-CoV in BALB/c mice by IMP dehydrogenase inhibitors, including ribavirin. Antiviral Res 2006b;71(1):53–63. [PubMed: 16621037]

Barnard DL, Hubbard VD, Burton J, Smee DF, Morrey JD, Otto MJ, Sidwell RW. Inhibition of severe acute respiratory syndrome-associated coronavirus (SARSCoV) by calpain inhibitors and beta-D-N4-hydroxycytidine. Antivir Chem Chemother 2004;15(1):15–22. [PubMed: 15074711]

Becker MM, Graham RL, Donaldson EF, Rockx B, Sims AC, Sheahan T, Pickles RJ, Corti D, Johnston RE, Baric RS, Denison MR. Synthetic recombinant bat SARS-like coronavirus is infectious in cultured cells and in mice. Proc Natl Acad Sci U S A 2008;105(50):19944–9. [PubMed: 19036930]

Cameron MJ, Bermejo-Martin JF, Danesh A, Muller MP, Kelvin DJ. Human immunopathogenesis of severe acute respiratory syndrome (SARS). Virus Res 2008;133(1):13–9. [PubMed: 17374415]

Carter WA, Pitha PM, Marshall LW, Tazawa I, Tazawa S, Ts'o PO. Structural requirements of the rI n -rC n complex for induction of human interferon. J Mol Biol 1972;70(3):567–87. [PubMed: 5083149]

Chen J, Subbarao K. The Immunobiology of SARS. Annual Review of Immunology 2007;25(1):443–472.

Cheung OY, Chan JW, Ng CK, Koo CK. The spectrum of pathological changes in severe acute respiratory syndrome (SARS). Histopathology 2004;45(2):119–24. [PubMed: 15279629]

Chowers MY, Lang R, Nassar F, Ben-David D, Giladi M, Rubinshtein E, Itzhaki A, Mishal J, Siegman-Igra Y, Kitzes R, Pick N, Landau Z, Wolf D, Bin H, Mendelson E, Pitlik SD, Weinberger M. Clinical characteristics of the West Nile fever outbreak, Israel, 2000. Emerg Infect Dis 2001;7(4):675–8. [PubMed: 11585531]

Chu YK, Ali GD, Jia F, Li Q, Kelvin D, Couch RC, Harrod KS, Hutt JA, Cameron C, Weiss SR, Jonsson CB. The SARS-CoV ferret model in an infection-challenge study. Virology 2008;374(1):151–163. [PubMed: 18234270]

Cinatl J, Morgenstern B, Bauer G, Chandra P, Rabenau H, Doerr HW. Treatment of SARS with human interferons. Lancet 2003;362(9380):293–4. [PubMed: 12892961]

De Clercq E. Current lead natural products for the chemotherapy of human immunodeficiency virus (HIV) infection. Med Res Rev 2000;20(5):323–49. [PubMed: 10934347]

Ding Y, He L, Zhang Q, Huang Z, Che X, Hou J, Wang H, Shen H, Qiu L, Li Z, Geng J, Cai J, Han H, Li X, Kang W, Weng D, Liang P, Jiang S. Organ distribution of severe acute respiratory syndrome (SARS) associated coronavirus (SARS-CoV) in SARS patients: implications for pathogenesis and virus transmission pathways. J Pathol 2004;203(2):622–30. [PubMed: 15141376]

Drosten C, Gunther S, Preiser W, van der Werf S, Brodt HR, Becker S, Rabenau H, Panning M, Kolesnikova L, Fouchier RA, Berger A, Burguiere AM, Cinatl J, Eickmann M, Escriou N, Grywna K, Kramme S, Manuguerra JC, Muller S, Rickerts V, Sturmer M, Vieth S, Klenk HD, Osterhaus AD, Schmitz H, Doerr HW. Identification of a novel coronavirus in patients with severe acute respiratory syndrome. N Engl J Med 2003a;348(20):1967–76. [PubMed: 12690091]

Drosten C, Preiser W, Gunther S, Schmitz H, Doerr HW. Severe acute respiratory syndrome: identification of the etiological agent. Trends Mol Med 2003b;9(8):325–7. [PubMed: 12928032]

Du L, He Y, Zhou Y, Liu S, Zheng BJ, Jiang S. The spike protein of SARS-CoV--a target for vaccine and therapeutic development. Nat Rev Microbiol 2009;7(3):226–36. [PubMed: 19198616]

Finter NB. Dye uptake methods for assessing viral cytopathogenicity and their application to interferon assays. J Gen Virol 1969;(5):419–427.

Fouchier RA, Kuiken T, Schutten M, van Amerongen G, van Doornum GJ, van den Hoogen BG, Peiris M, Lim W, Stohr K, Osterhaus AD. Aetiology: Koch's postulates fulfilled for SARS virus. Nature 2003;423(6937):240. [PubMed: 12748632]

Franks TJ, Chong PY, Chui P, Galvin JR, Lourens RM, Reid AH, Selbs E, McEvoy CP, Hayden CD, Fukuoka J, Taubenberger JK, Travis WD. Lung pathology of severe acute respiratory syndrome (SARS): a study of 8 autopsy cases from Singapore. Hum Pathol 2003;34(8):743–8. [PubMed: 14506633]

Frieman M, Heise M, Baric R. SARS coronavirus and innate immunity. Virus Res 2008;133(1):101–12. [PubMed: 17451827]

Glass WG, Subbarao K, Murphy B, Murphy PM. Mechanisms of host defense following severe acute respiratory syndrome-coronavirus (SARS-CoV) pulmonary infection of mice. J Immunol 2004;173(6):4030–9. [PubMed: 15356152]

Gowen BB, Hoopes JD, Wong MH, Jung KH, Isakson KC, Alexopoulou L, Flavell RA, Sidwell RW. TLR3 deletion limits mortality and disease severity due to Phlebovirus infection. J Immunol 2006;177(9):6301–7. [PubMed: 17056560]

Gowen BB, Wong MH, Jung KH, Sanders AB, Mitchell WM, Alexopoulou L, Flavell RA, Sidwell RW. TLR3 is essential for the induction of protective immunity against Punta Toro Virus infection by the

double-stranded RNA (dsRNA), poly(I:C12U), but not Poly(I:C): differential recognition of synthetic dsRNA molecules. J Immunol 2007;178(8):5200–8. [PubMed: 17404303]

Greenough TC, Carville A, Coderre J, Somasundaran M, Sullivan JL, Luzuriaga K, Mansfield K. Pneumonitis and multi-organ system disease in common marmosets (Callithrix jacchus) infected with the severe acute respiratory syndrome-associated coronavirus. Am J Pathol 2005;167(2):455–63. [PubMed: 16049331]

Guan Y, Zheng BJ, He YQ, Liu XL, Zhuang ZX, Cheung CL, Luo SW, Li PH, Zhang LJ, Guan YJ, Butt KM, Wong KL, Chan KW, Lim W, Shortridge KF, Yuen KY, Peiris JS, Poon LL. Isolation and characterization of viruses related to the SARS coronavirus from animals in southern China. Science 2003;302(5643):276–8. [PubMed: 12958366]

Guo Y, Korteweg C, McNutt MA, Gu J. Pathogenetic mechanisms of severe acute respiratory syndrome. Virus Res 2008;133(1):4–12. [PubMed: 17825937]

Hegde S, Pahne J, Smola-Hess S. Novel immunosuppressive properties of interleukin-6 in dendritic cells: inhibition of NF-kappaB binding activity and CCR7 expression. FASEB J 2004;18(12):1439–41. [PubMed: 15247147]

Hon CC, Lam TY, Shi ZL, Drummond AJ, Yip CW, Zeng F, Lam PY, Leung FC. Evidence of the recombinant origin of a bat severe acute respiratory syndrome (SARS)-like coronavirus and its implications on the direct ancestor of SARS coronavirus. J Virol 2008;82(4):1819–26. [PubMed: 18057240]

Hsiao CH, Wu MZ, Chen CL, Hsueh PR, Hsieh SW, Yang PC, Su IJ. Evolution of pulmonary pathology in severe acute respiratory syndrome. J Formos Med Assoc 2005;104(2):75–81. [PubMed: 15765160]

Hsueh PR, Chen PJ, Hsiao CH, Yeh SH, Cheng WC, Wang JL, Chiang BL, Chang SC, Chang FY, Wong WW, Kao CL, Yang PC. Patient data, early SARS epidemic, Taiwan. Emerg Infect Dis 2004;10(3):489–93. [PubMed: 15109419]

Huang YH, Lei HY, Liu HS, Lin YS, Liu CC, Yeh TM. Dengue virus infects human endothelial cells and induces IL-6 and IL-8 production. Am J Trop Med Hyg 2000;63(1–2):71–5. [PubMed: 11357999]

Hultgren C, Milich DR, Weiland O, Sallberg M. The antiviral compound ribavirin modulates the T helper (Th) 1/Th2 subset balance in hepatitis B and C virus-specific immune responses. J Gen Virol 1998;79 (Pt 10):2381–91. [PubMed: 9780043]

Jiang Y, Xu J, Zhou C, Wu Z, Zhong S, Liu J, Luo W, Chen T, Qin Q, Deng P. Characterization of Cytokine/Chemokine Profiles of Severe Acute Respiratory Syndrome. Am J Respir Crit Care Med 2005;171(8):850–857. [PubMed: 15657466]

Jiang Z, Kunimoto M, Patel JA. Autocrine regulation and experimental modulation of interleukin-6 expression by human pulmonary epithelial cells infected with respiratory syncytial virus. J Virol 1998;72(3):2496–9. [PubMed: 9499112]

Jones BM, Ma ES, Peiris JS, Wong PC, Ho JC, Lam B, Lai KN, Tsang KW. Prolonged disturbances of in vitro cytokine production in patients with severe acute respiratory syndrome (SARS) treated with ribavirin and steroids. Clin Exp Immunol 2004;135(3):467–73. [PubMed: 15008980]

Julander JG, Skirpstunas R, Siddharthan V, Shafer K, Hoopes JD, Smee DF, Morrey JD. C3H/HeN mouse model for the evaluation of antiviral agents for the treatment of Venezuelan equine encephalitis virus infection. Antiviral Res 2008;78(3):230–41. [PubMed: 18313150]

Keyaerts E, Vijgen L, Pannecouque C, Van Damme E, Peumans W, Egberink H, Balzarini J, Van Ranst M. Plant lectins are potent inhibitors of coronaviruses by interfering with two targets in the viral replication cycle. Antiviral Res 2007;75(3):179–87. [PubMed: 17428553]

Kopf M, Baumann H, Freer G, Freudenberg M, Lamers M, Kishimoto T, Zinkernagel R, Bluethmann H, Kohler G. Impaired immune and acute-phase responses in interleukin-6-deficient mice. Nature 1994;368(6469):339–42. [PubMed: 8127368]

Ksiazek TG, Erdman D, Goldsmith CS, Zaki SR, Peret T, Emery S, Tong S, Urbani C, Comer JA, Lim W, Rollin PE, Dowell SF, Ling AE, Humphrey CD, Shieh WJ, Guarner J, Paddock CD, Rota P, Fields B, DeRisi J, Yang JY, Cox N, Hughes JM, LeDuc JW, Bellini WJ, Anderson LJ. A novel coronavirus associated with severe acute respiratory syndrome. N Engl J Med 2003;348(20):1953–66. [PubMed: 12690092]

Kumaki Y, Day CW, Wandersee MK, Schow BP, Madsen JS, Grant D, Roth JP, Smee DF, Blatt LM, Barnard DL. Interferon alfacon 1 inhibits SARS-CoV infection in human bronchial epithelial Calu-3 cells. Biochem Biophys Res Commun 2008;371(1):110–3. [PubMed: 18406349]

Kuri T, Zhang X, Habjan M, Martinez-Sobrido L, Garcia-Sastre A, Yuan Z, Weber F. Interferon priming enables cells to partially overturn the SARS-Coronavirus-induced block in innate immune activation. J Gen Virol. 2009

Kurt-Jones EA, Belko J, Yu C, Newburger PE, Wang J, Chan M, Knipe DM, Finberg RW. The role of toll-like receptors in herpes simplex infection in neonates. J Infect Dis 2005;191(5):746–8. [PubMed: 15688290]

Lang Z, Zhang L, Zhang S, Meng X, Li J, Song C, Sun L, Zhou Y. Pathological study on severe acute respiratory syndrome. Chin Med J (Engl) 2003;116(7):976–80. [PubMed: 12890365]

Leyssen P, Drosten C, Paning M, Charlier N, Paeshuyse J, De Clercq E, Neyts J. Interferons, interferon inducers, and interferon-ribavirin in treatment of flavivirus-induced encephalitis in mice. Antimicrob Agents Chemother 2003;47(2):777–82. [PubMed: 12543691]

Li F, Li W, Farzan M, Harrison SC. Structure of SARS coronavirus spike receptor-binding domain complexed with receptor. Science 2005a;309(5742):1864–8. [PubMed: 16166518]

Li W, Moore MJ, Vasilieva N, Sui J, Wong SK, Berne MA, Somasundaran M, Sullivan JL, Luzuriaga K, Greenough TC, Choe H, Farzan M. Angiotensin-converting enzyme 2 is a functional receptor for the SARS coronavirus. Nature 2003;426(6965):450–4. [PubMed: 14647384]

Li W, Shi Z, Yu M, Ren W, Smith C, Epstein JH, Wang H, Crameri G, Hu Z, Zhang H, Zhang J, McEachern J, Field H, Daszak P, Eaton BT, Zhang S, Wang LF. Bats are natural reservoirs of SARS-like coronaviruses. Science 2005b;310(5748):676–9. [PubMed: 16195424]

Martina BE, Haagmans BL, Kuiken T, Fouchier RA, Rimmelzwaan GF, Van Amerongen G, Peiris JS, Lim W, Osterhaus AD. Virology: SARS virus infection of cats and ferrets. Nature 2003;425(6961): 915. [PubMed: 14586458]

McManus NH. Microtiter assay for interferon: microspectrophotometric quantitation of cytopathic effect. Appl Environ Microbiol 1976;31(1):35–8. [PubMed: 182074]

McRoy WC, Baric RS. Amino acid substitutions in the S2 subunit of mouse hepatitis virus variant V51 encode determinants of host range expansion. J Virol 2008;82(3):1414–24. [PubMed: 18032498]

Morgenstern B, Michaelis M, Baer PC, Doerr HW, Cinatl J Jr. Ribavirin and interferon-beta synergistically inhibit SARS-associated coronavirus replication in animal and human cell lines. Biochem Biophys Res Commun 2005;326(4):905–8. [PubMed: 15607755]

Morrey JD, Day CW, Julander JG, Blatt LM, Smee DF, Sidwell RW. Effect of interferon-alpha and interferon-inducers on West Nile virus in mouse and hamster animal models. Antivir Chem Chemother 2004;15(2):101–9. [PubMed: 15185728]

Nagata N, Iwata N, Hasegawa H, Fukushi S, Harashima A, Sato Y, Saijo M, Taguchi F, Morikawa S, Sata T. Mouse-Passaged Severe Acute Respiratory Syndrome-Associated Coronavirus Leads to Lethal Pulmonary Edema and Diffuse Alveolar Damage in Adult but Not Young Mice. Am J Pathol 2008;172(6):1625–1637. [PubMed: 18467696]

Nagata N, Iwata N, Hasegawa H, Fukushi S, Yokoyama M, Harashima A, Sato Y, Saijo M, Morikawa S, Sata T. Participation of both host and virus factors in induction of severe acute respiratory syndrome (SARS) in F344 rats infected with SARS coronavirus. J Virol 2007;81(4):1848–57. [PubMed: 17151094]

Nicholls JM, Poon LL, Lee KC, Ng WF, Lai ST, Leung CY, Chu CM, Hui PK, Mak KL, Lim W, Yan KW, Chan KH, Tsang NC, Guan Y, Yuen KY, Peiris JS. Lung pathology of fatal severe acute respiratory syndrome. Lancet 2003;361(9371):1773–8. [PubMed: 12781536]

Niu J, Wang Y, Dixon R, Bowden S, Qiao M, Einck L, Locarnini S. The use of ampligen alone and in combination with ganciclovir and coumermycin A1 for the treatment of ducks congenitally-infected with duck hepatitis B virus. Antiviral Res 1993;21(2):155–71. [PubMed: 7687840]

Pacciarini F, Ghezzi S, Canducci F, Sims A, Sampaolo M, Ferioli E, Clementi M, Poli G, Conaldi PG, Baric R, Vicenzi E. Persistent replication of severe acute respiratory syndrome coronavirus in human tubular kidney cells selects for adaptive mutations in the membrane protein. J Virol 2008;82(11): 5137–44. [PubMed: 18367528]

Padalko E, Nuyens D, De Palma A, Verbeken E, Aerts JL, De Clercq E, Carmeliet P, Neyts J. The interferon inducer ampligen [poly(I)-poly(C12U)] markedly protects mice against coxsackie B3 virus-induced myocarditis. Antimicrob Agents Chemother 2004;48(1):267–74. [PubMed: 14693549]

Peiris JSM, Chu CM, Cheng VCC, Chan KS, Hung IFN, Poon LLM, Law KI, Tang BSF, Hon TYW, Chan CS, Chan KH, Ng JSC, Zheng BJ, Ng WL, Lai RWM, Guan Y, Yuen KY. Clinical progression and viral load in a community outbreak of coronavirus-associated SARS pneumonia: a prospective study. The Lancet 2003a;361(9371):1767–1772.

Peiris JSM, Lai ST, Poon LLM, Guan Y, Yam LYC, Lim W, Nicholls J, Yee WKS, Yan WW, Cheung MT, Cheng VCC, Chan KH, Tsang DNC, Yung RWH, Ng TK, Yuen KY. Coronavirus as a possible cause of severe acute respiratory syndrome. The Lancet 2003b;361(9366):1319–1325.

Perlman S, Dandekar AA. Immunopathogenesis of coronavirus infections: implications for SARS. Nat Rev Immunol 2005;5(12):917–27. [PubMed: 16322745]

Pinto AJ, Morahan PS, Brinton MA. Comparative study of various immunomodulators for macrophage and natural killer cell activation and antiviral efficacy against exotic RNA viruses. Int J Immunopharmacol 1988;10(3):197–209. [PubMed: 3182149]

Pyrc K, Berkhout B, van der Hoek L. Antiviral strategies against human coronaviruses. Infect Disord Drug Targets 2007;7(1):59–66. [PubMed: 17346212]

Reed LJ, Muench M. A simple method of estimating fifty percent end points. Am J Hyg 1938;(27):493–498.

Roberts A, Deming D, Paddock CD, Cheng A, Yount B, Vogel L, Herman BD, Sheahan T, Heise M, Genrich GL, Zaki SR, Baric R, Subbarao K. A Mouse-Adapted SARS-Coronavirus Causes Disease and Mortality in BALB/c Mice. PLoS Pathogens 2007;3(1):e5. [PubMed: 17222058]

Roberts A, Paddock C, Vogel L, Butler E, Zaki S, Subbarao K. Aged BALB/c mice as a model for increased severity of severe acute respiratory syndrome in elderly humans. J Virol 2005;79(9):5833–8. [PubMed: 15827197]

Roberts A, Subbarao K. Animal models for SARS. Adv Exp Med Biol 2006;581:463–71. [PubMed: 17037579]

Roberts A, Thomas WD, Guarner J, Lamirande EW, Babcock GJ, Greenough TC, Vogel L, Hayes N, Sullivan JL, Zaki S, Subbarao K, Ambrosino DM. Therapy with a Severe Acute Respiratory Syndrome-Associated Coronavirus-Neutralizing Human Monoclonal antibody Reduces Disease Severity and Viral Burden in Golden Syrian Hamsters. J Infect Dis 2006;193:685–692. [PubMed: 16453264]

Rockx B, Sheahan T, Donaldson E, Harkema J, Sims A, Heise M, Pickles R, Cameron M, Kelvin D, Baric R. Synthetic reconstruction of zoonotic and early human severe acute respiratory syndrome coronavirus isolates that produce fatal disease in aged mice. J Virol 2007;81(14):7410–23. [PubMed: 17507479]

Sadler AJ, Williams BR. Interferon-inducible antiviral effectors. Nat Rev Immunol 2008;8(7):559–68. [PubMed: 18575461]

Samuel CE. Antiviral actions of interferons. Clin Microbiol Rev 2001;14(4):778–809. [PubMed: 11585785]table of contents

Sheahan T, Rockx B, Donaldson E, Sims A, Pickles R, Corti D, Baric R. Mechanisms of zoonotic severe acute respiratory syndrome coronavirus host range expansion in human airway epithelium. J Virol 2008;82(5):2274–85. [PubMed: 18094188]

Sidwell RW, Huffman JH. Use of disposable micro tissue culture plates for antiviral and interferon induction studies. Appl Microbiol 1971;22(5):797–801. [PubMed: 4332040]

Sidwell RW, Huffman JH, Barnard DL, Smee DF, Warren RP, Chirigos MA, Kende M, Huggins J. Antiviral and immunomodulating inhibitors of experimentally-induced Punta Toro virus infections. Antiviral Res 1994;25(2):105–22. [PubMed: 7847873]

Sidwell RW, Huffman JH, Khare GP, Allen LB, Witkowski JT, Robins RK. Broad-spectrum antiviral activity of Virazole: 1-beta-D-ribofuranosyl-1,2,4-triazole-3-carboxamide. Science 1972;177(50):705–6. [PubMed: 4340949]

Smee DF, Gilbert J, Leonhardt JA, Barnett BB, Huggins JH, Sidwell RW. Treatment of lethal Pichinde virus infections in weanling LVG/Lak hamsters with ribavirin, ribamidine, selenazofurin, and ampligen. Antiviral Res 1993;20(1):57–70. [PubMed: 8384433]

Smee DF, Morris JL, Leonhardt JA, Mead JR, Holy A, Sidwell RW. Treatment of murine cytomegalovirus infections in severe combined immunodeficient mice with ganciclovir, (S)-1-[3-hydroxy-2-(phosphonylmethoxy)propyl]cytosine, interferon, and bropirimine. Antimicrob Agents Chemother 1992;36(9):1837–42. [PubMed: 1329629]

Stockman LJ, Bellamy R, Garner P. SARS: systematic review of treatment effects. PLoS Med 2006;3 (9):e343. [PubMed: 16968120]

Streeter DG, Witkowski JT, Khare GP, Sidwell RW, Bauer RJ, Robins RK, Simon LN. Mechanism of action of 1- -D-ribofuranosyl-1,2,4-triazole-3-carboxamide (Virazole), a new broad-spectrum antiviral agent. Proc Natl Acad Sci U S A 1973;70(4):1174–8. [PubMed: 4197928]

Stroher U, DiCaro A, Li Y, Strong JE, Aoki F, Plummer F, Jones SM, Feldmann H. Severe acute respiratory syndrome-related coronavirus is inhibited by interferon- alpha. J Infect Dis 2004;189(7): 1164–7. [PubMed: 15031783]

Subbarao K, Roberts A. Is there an ideal animal model for SARS? Trends in Microbiology 2006;14(7): 299–303. [PubMed: 16759866]

Tong TR. Therapies for coronaviruses. Part 2: Inhibitors of intracellular life cycle. Expert Opin Ther Pat 2009a;19(4):415–31. [PubMed: 19441924]

Tong TR. Therapies for coronaviruses. Part I of II -- viral entry inhibitors. Expert Opin Ther Pat 2009b; 19(3):357–67. [PubMed: 19449500]

van den Brand JM, Haagmans BL, Leijten L, van Riel D, Martina BE, Osterhaus AD, Kuiken T. Pathology of experimental SARS coronavirus infection in cats and ferrets. Vet Pathol 2008;45(4):551–62. [PubMed: 18587105]

van der Meer FJ, de Haan CA, Schuurman NM, Haijema BJ, Peumans WJ, Van Damme EJ, Delputte PL, Balzarini J, Egberink HF. Antiviral activity of carbohydrate-binding agents against Nidovirales in cell culture. Antiviral Res 2007a;76(1):21–9. [PubMed: 17560666]

van der Meer FJ, de Haan CA, Schuurman NM, Haijema BJ, Verheije MH, Bosch BJ, Balzarini J, Egberink HF. The carbohydrate-binding plant lectins and the non-peptidic antibiotic pradimicin A target the glycans of the coronavirus envelope glycoproteins. J Antimicrob Chemother 2007b;60(4): 741–9. [PubMed: 17704516]

Wang CH, Liu CY, Wan YL, Chou CL, Huang KH, Lin HC, Lin SM, Lin TY, Chung K, Kuo HP. Persistence of lung inflammation and lung cytokines with high-resolution CT abnormalities during recovery from SARS. Respiratory Research 2005;6(1):42. [PubMed: 15888207]

Wang WK, Chen SY, Liu IJ, Kao CL, Chen HL, Chiang BL, Wang JT, Sheng WH, Hsueh PR, Yang CF, Yang PC, Chang SC. Temporal Relationship of Viral Load, Ribavirin, Interleukin (IL)-6, IL-8, and Clinical Progression in Patients with Severe Acute Respiratory Syndrome. Clinical Infectious Diseases 2004;39(7):1071–1075. [PubMed: 15472864]

Wong SS, Yuen KY. The management of coronavirus infections with particular reference to SARS. J Antimicrob Chemother 2008;62(3):437–41. [PubMed: 18565970]

Wu YS, Lin WH, Hsu JT, Hsieh HP. Antiviral drug discovery against SARS-CoV. Curr Med Chem 2006;13(17):2003–20. [PubMed: 16842194]

Ye J, Zhang B, Xu J, Chang Q, McNutt MA, Korteweg C, Gong E, Gu J. Molecular pathology in the lungs of severe acute respiratory syndrome patients. Am J Pathol 2007;170(2):538–45. [PubMed: 17255322]

Yeung KS, Meanwell NA. Recent developments in the virology and antiviral research of severe acute respiratory syndrome coronavirus. Infect Disord Drug Targets 2007;7(1):29–41. [PubMed: 17346209]

Zhang HZ, Zhang H, Kemnitzer W, Tseng B, Cinatl J Jr, Michaelis M, Doerr HW, Cai SX. Design and synthesis of dipeptidyl glutaminyl fluoromethyl ketones as potent severe acute respiratory syndrome coronovirus (SARS-CoV) inhibitors. J Med Chem 2006;49(3):1198–201. [PubMed: 16451084]

Zhu M. SARS Immunity and Vaccination. Cell Mol Immunol 2004;1(3):193–8. [PubMed: 16219167]

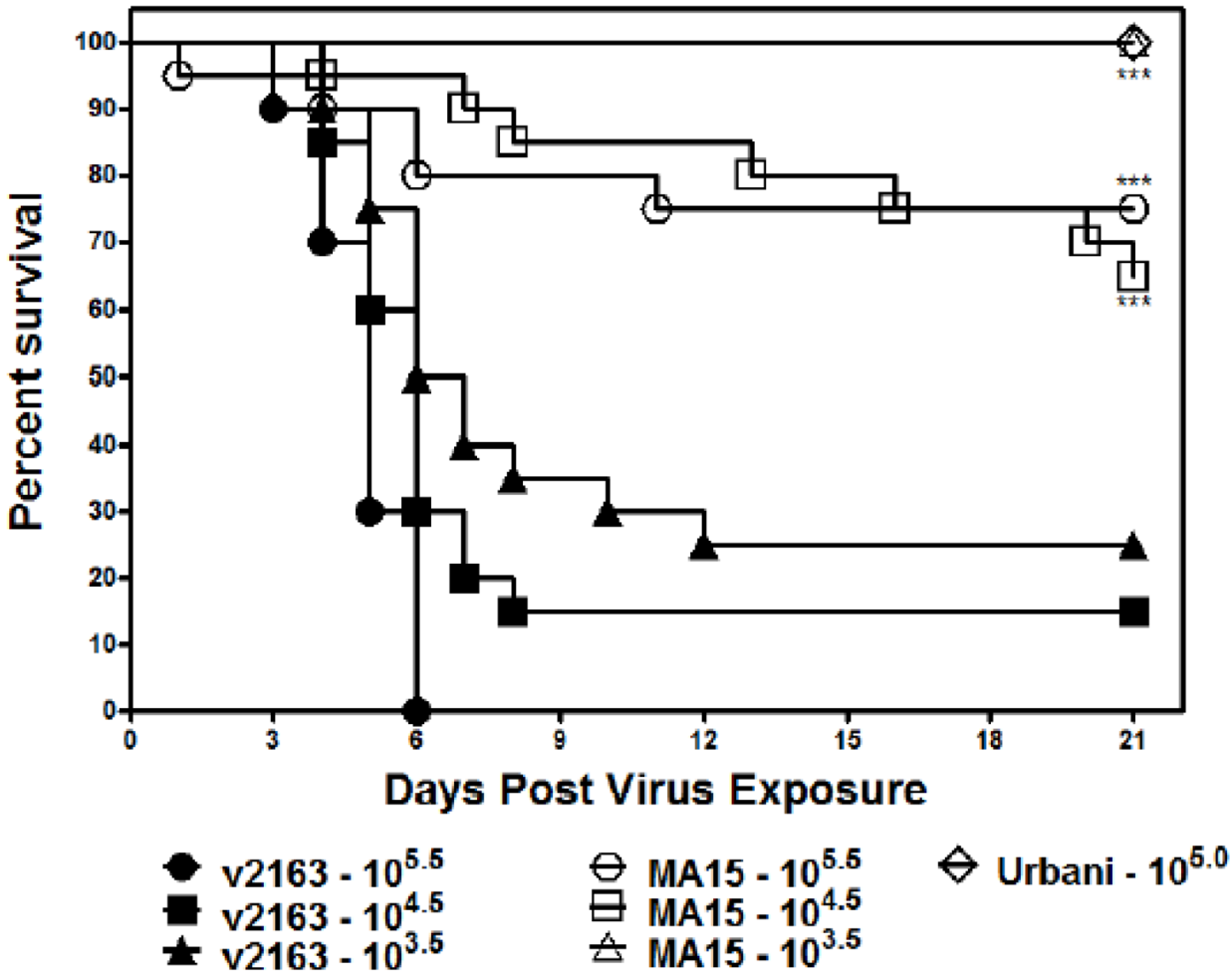

Figure 1.
Percent survival of 5–6 week old BALB/c mice infected with SARS-CoV strains Urbani, v2163, and MA15. $^{***}P < 0.001$ MA15 compared with v2163.

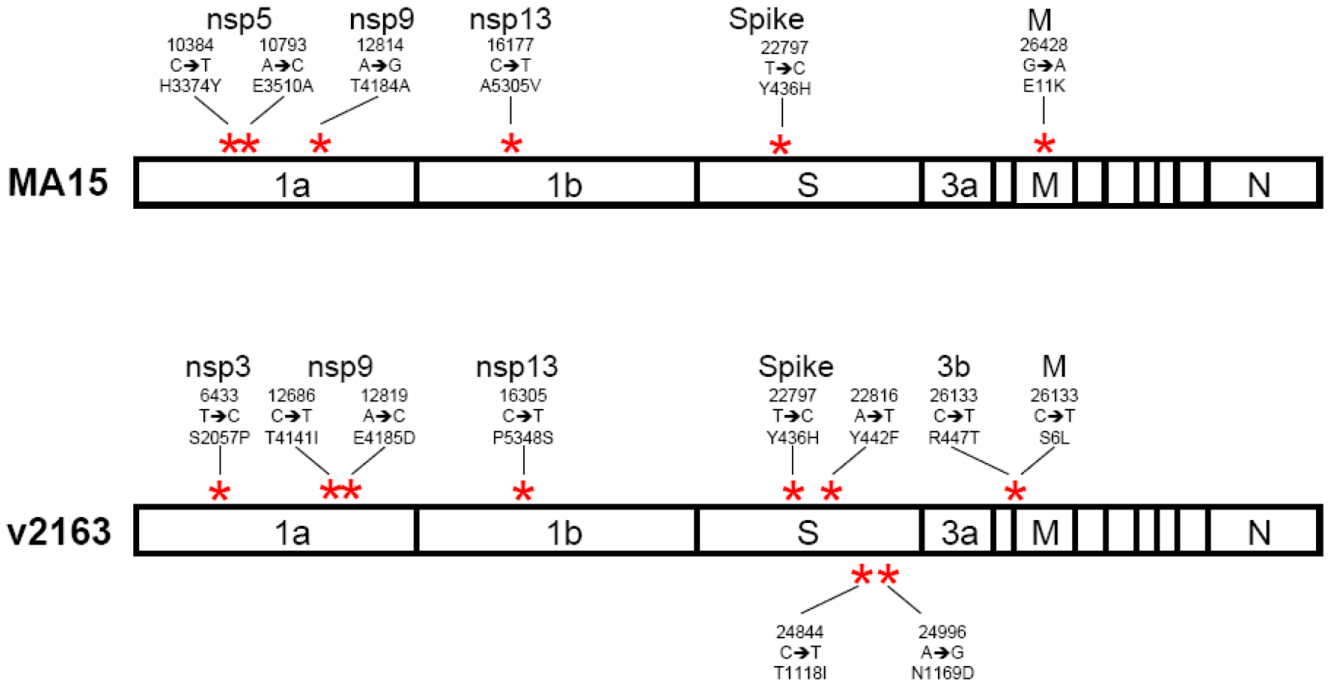

Figure 2.
Mutations found in v2163 and MA15 mouse-adapted strains of SARS-CoV compared with the Urbani strain.

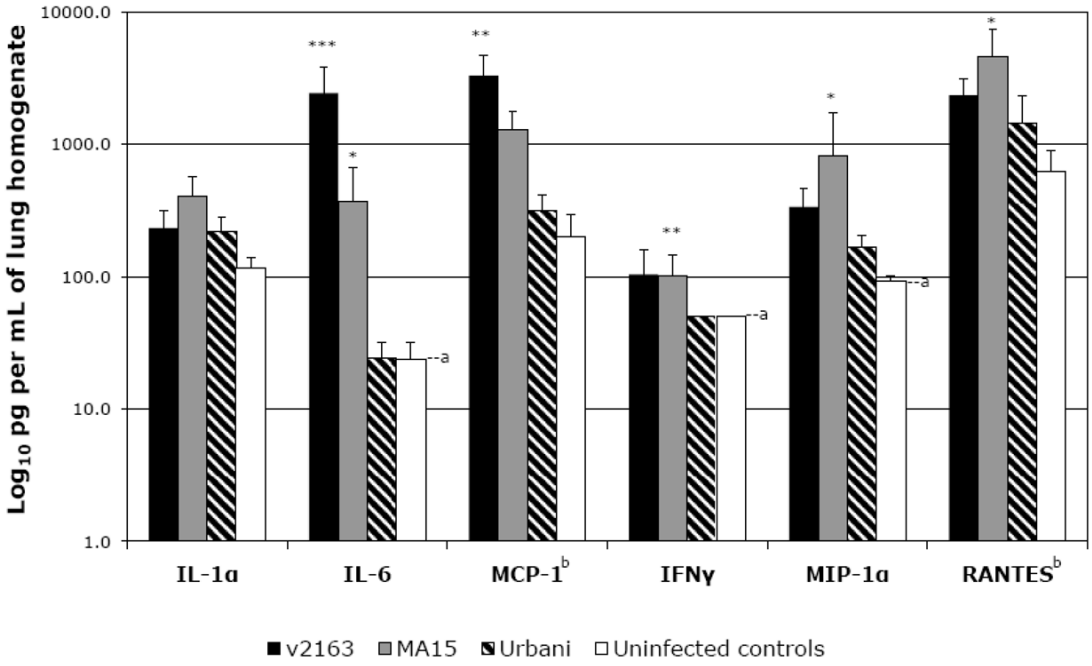

Figure 3.

Average cytokines detected in BALB/c mice lungs 3 days after infection with various strains of SARS-CoV ($n \geq 8$). Black bars are v2163, gray bars are MA15, striped bars are Urbani, and white bars are uninfected controls. *$P < 0.05$, **$P < 0.01$, ***$P < 0.001$ MA15 compared with Urbani.

[a]Lower limit of detection

[b]The v2163 and MA15 averages included some extrapolated values that were minimum estimates.

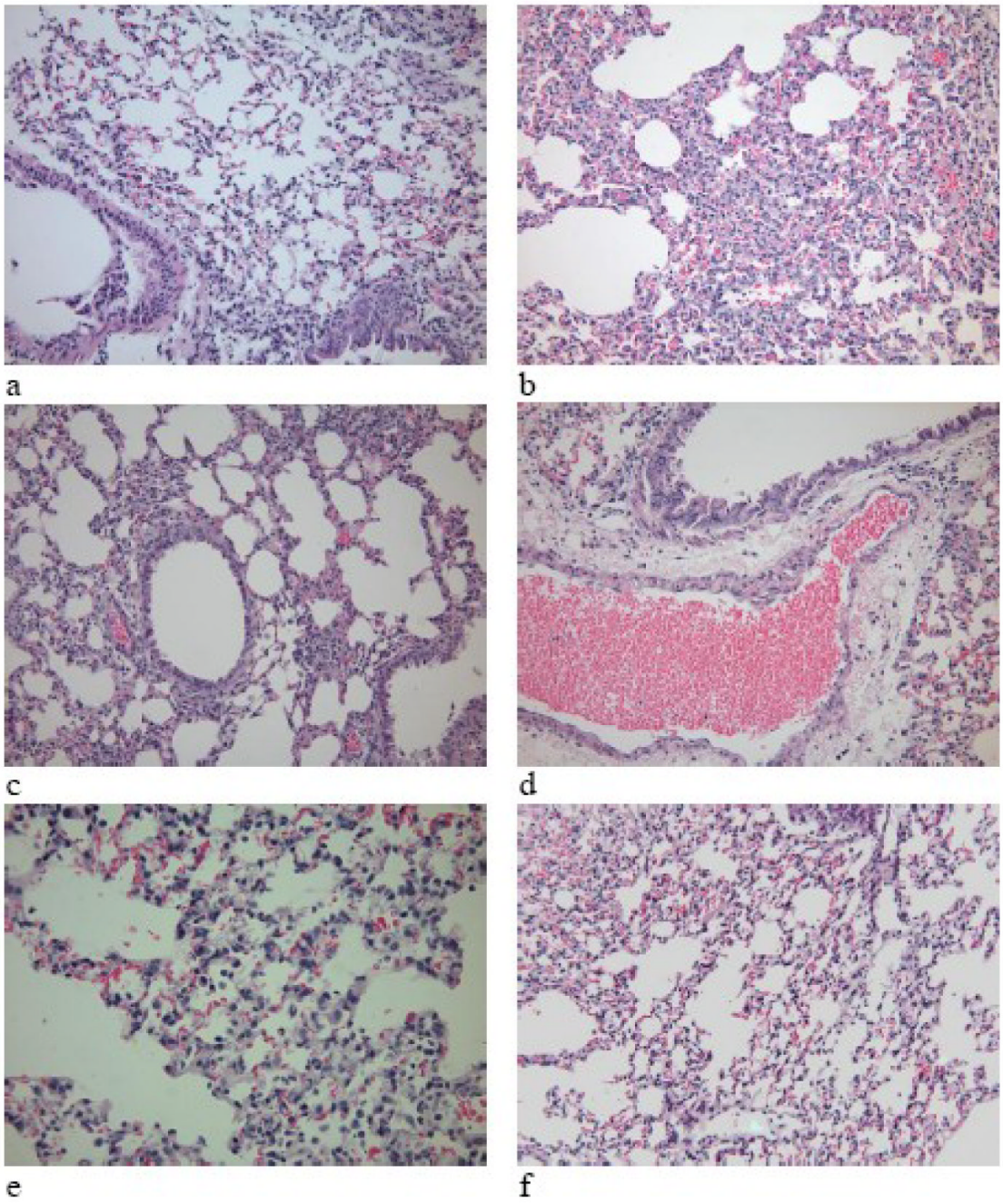

Figure 4.
Histological slides showing representative lung pathology; a) Urbani- infected lung with no significant changes (40×); b) MA15-infected lung with small numbers of foamy macrophages that widen scattered alveolar septae (40×), c) MA15-infected lung with rare individual bronchiolar lining cells that were swollen and hypereosinophilic, and scattered alveolar septae widened by foamy macrophages (40×), d) v2163-infected lung with moderate numbers of neutrophils and edema fluid surrounding several large vessels (40×), e) v2163-infected lung with small numbers of alveolar macrophages throughout airspaces (60×), and f) uninfected lung with no significant changes (40×).

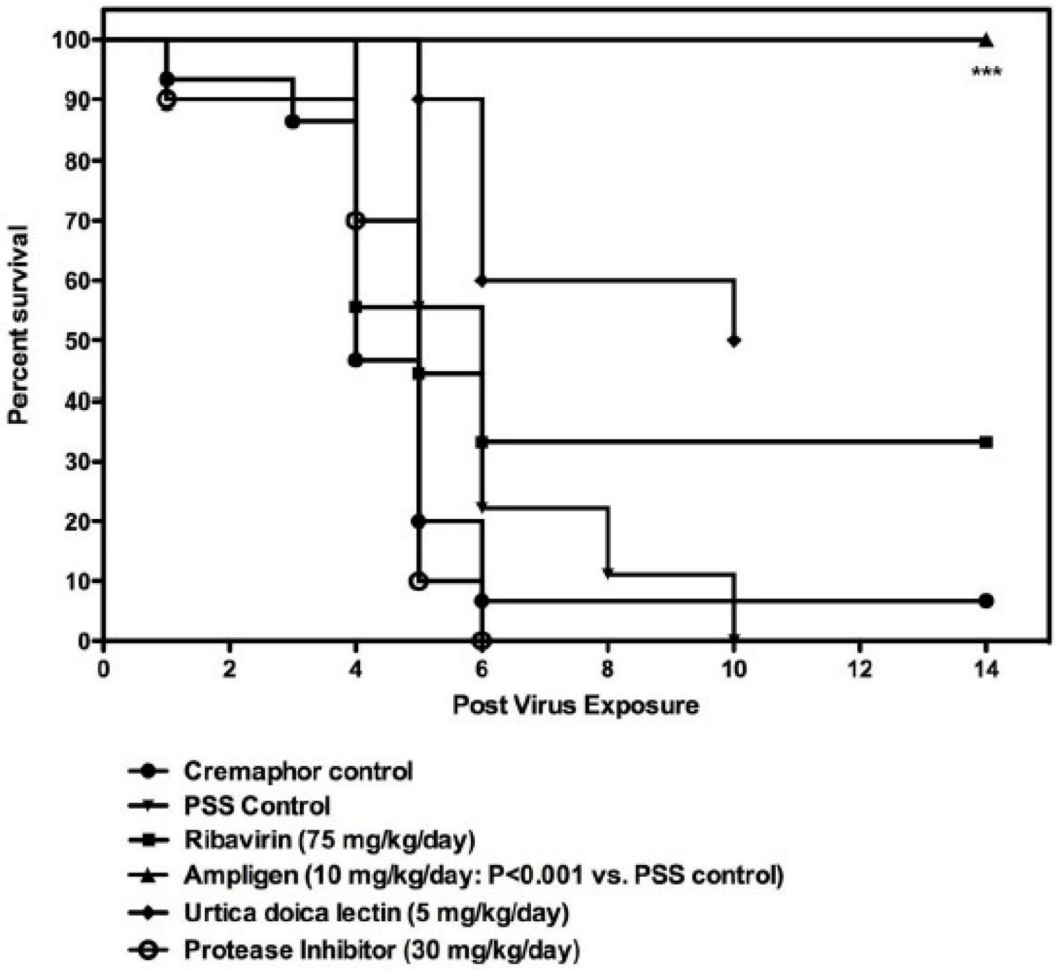

Figure 5.
Effects of Ampligen™, ribavirin, EP128533, and UDA on survival of BALB/c mice infected with SARS-CoV strain v2163.

Table 1

Mortality, lung virus titer, and weight loss of 5–6 week old BALB/c mice infected intranasally with the Urbani strain and two mouse-adapted strains of SARS-CoV.

SARS Strain	Inoculum (~$CCID_{50}$)	Survivors	Mice losing 20% of Weight	% Weight Change 4 dpi	Lung Titer 3 dpi (Log $CCID_{50}$/g)	Lung Titer 6 dpi (Log $CCID_{50}$/g)
v2163	$10^{5.5}$	0/10	10/10	−24 ± 5.7	7.4 ± 1.1	nt[a]
v2163	$10^{4.5}$	2/10	10/10	−23 ± 1.1	7.8 ± 0.3	6.2 ± 2.6
v2163	$10^{3.5}$	3/10	10/10	−24 ± 4.9	7.9 ± 0.3	7.3 ± 0.6
MA15	$10^{5.5}$	7/10**	9/10	−22 ± 8.3	6.6 ± 0.3	nt[a]
MA15	$10^{4.5}$	9/10**	8/10	−21 ± 3.0	6.7 ± 0.1*	4.8 ± 1.1[b]
MA15	$10^{3.5}$	10/10**	4/10	−19 ± 3.3	6.9 ± 0.2	6.3 ± 0.7
Urbani	$10^{5.0}$	10/10	0/10	2.2 ± 8.5	5.8 ± 1.1	<3.8
Uninfected	None	5/5	0/10	1.3 ± 4.1	<3.8	<3.8

*P < 0.05,

**P < 0.01 for MA15 compared with corresponding dilution of v2163

[a]Not tested due to early death at this virus concentration

[b]Average contains one value below the limit of detection

Table 2

Death and weight comparisons of 5–6 week and 10–11 week old BALB/c mice infected intranasally with v2163, MA15, or Urbani strains of SARS-CoV.

SARS Strain	Inoculum (~$CCID_{50}$)	5–6 week old mice			10–11 week old mice		
		% Weight Change (4 dpi)	Survival	MDD[b]	% Weight Change (4 dpi)	Survival	MDD[a]
v2163	$10^{5.5}$	−24 ± 3.6	0/10	4.5 ± 0.7	−18 ± 1.2	0/10	4.8 ± 1.8
v2163	$10^{4.5}$	−23 ± 3.8	1/10	5.9 ± 1.4	−17 ± 5.0	1/10	5.7 ± 1.0
v2163	$10^{3.5}$	−26 ± 3.1	2/10	6.4 ± 1.9	−20 ± 2.0	0/10	7.3 ± 0.7
MA15	$10^{5.5}$	−25 ± 3.5	8/10*	3.5 ± 3.5	−22 ± 2.1	1/10	6.8 ± 1.4
MA15	$10^{4.5}$	−28 ± 1.6**	4/10	13.5 ± 6.9	−23 ± 2.4***	3/10	8.6 ± 3.9
MA15	$10^{3.5}$	−23 ± 3.4	10/10***	N/A	−24 ± 1.4*	9/10***	14 (n = 1)
Urbani	$10^{5.0}$	−0.5 ± 2.3	10/10	N/A	−2.3 ± 2.2	10/10	N/A
Uninfected	None	0 ± 2.4	5/5	N/A	−2.3 ± 2.5	5/5	N/A

*P < 0.05,

***P < 0.001 MA15 compared with corresponding dilution of v2163

[a]Mean day of death; animals surviving to the end of the study were excluded

Table 3

Survival, mean day of death, lung scores, weight change, and virus titers in BALB/c mice infected with mouse-adapted SARS-CoV v2163 and treated with ribavirin or Ampligen™.

Treatment	Survivors/Total	Mean Day of Death ± SD	Lung score 6 dpi	Weight change (grams)[a]	Lung Titer 3 dpi (Log $CCID_{50}$/g)	Lung Titer 6 dpi (Log $CCID_{50}$/g)
Normal Saline	0/10	6.2 ± 1.7	3.2 ± 0.58	−3.4 ± 2.7	7.0 ± 0.11	5.9 ± 1.4
Ribavirin 75 mg/kg/day	3/10	4.5 ± 0.84*	2.5 ± 0.94	−1.6 ± 1.4*	7.0 ± 0.24	7.0 ± 0.82
Ampligen™10 mg/kg/day	10/10***	>14***	0.90 ± 0.89*	0.50 ± 0.78***	7.6 ± 0.52	4.3 ± 0.16
UDA[b] 5 mg/kg/day	5/10*	6.6 ± 2.0	2.17±0.29	−2.3 ± 0.14	7.32± .07	6.6 ± 0.93
Cremaphor[c]	1/15	4.3 ± 1.3	NT	−2.6 ± 0.35	8.1 ± 0.23	NT
EP128533[c] 30 mg/kg/day	0/10	4.5 ± 1.4	NT	−3.2 ± 0.28	8.2 ± 0.14	NT

*P< 0.05,

***P<0.001 compared with saline or cremaphor control NT = not tested, all mice died before day 6

[a]Mean weight difference evaluated on day 3 post virus exposure

[b]Separate experiment with 10 day duration versus normal 21 days

[c]Separate experiment with 10% cremaphor as diluent instead of saline

Table 4

Lung IL-6 levels and pathology in BALB/c mice 3 days and 6 days after infection with SARS-CoV strain v2163 and treatment with Ampligen™, ribavirin, UDA, or EP128533.

Treatment	Day[a]	IL-6 (pg/mL)	Lung Titer (Log $CCID_{50}$/g)	Summary of Histopathology (inclusive)			
				Neutrophils[b]	Histiocytes[c]	Widened Alveoli[d]	Degenerate/Necrotic[e]
Saline, Uninfected	3	2200 ± 670	<2.8	0	0	0	0
Saline	3	3880 ± 2210	7.7 ± 0.63	3	3	2	3
Ribavirin (75 mg/kg/d)	3	2230 ± 610*	7.7 ± 0.21	2	2	2	1
Ampligen™ (10 mg/kg/d)	3	1650 ± 580*	8.0 ± 0.39	3	3	3	0
UDA (5 mg/kg/d)	3	3330 ± 1340	7.9 ± 0.84	3	3	3	2
EP128533 (30 mg/kg/d)	3	4690 ± 1520	8.2 ± 0.14	0	1	0	1
Cremaphor control	3	5000 ± 1990	8.1 ± 0.23	1	1	1	1
Saline Control	6	2140 ± 560	6.8 ± 0.85	2	2	1	0
Ribavirin (75 mg/kg/d)	6	2320 ± 820	5.0 ± 1.7	0	2	0	0
Ampligen™ (10 mg/kg/d)	6	1590 ± 380	6.2 ± 1.5	3	3	3	0
UDA (5 mg/kg/d)	6	2530 ± 1760	7.0 ± 0.32	3	3	3	0
EP128533 (30 mg/kg/d)	6	nt	nt	nt	nt	nt	nt
Cremaphor control	6	nt	nt	nt	nt	nt	nt

*P < 0.05,

**P < 0.01, by Wilcoxon analysis compared to untreated control (excluding 655 pg/mL outlier in PSS day 3) nt = not tested because all mice from this group died before day 6

[a]Days post inoculation

[b]Small to moderate numbers of neutrophils in alveoli or surrounding scattered vessels

[c]Small to moderate numbers of histiocytes in alveoli

[d]Widened groups of alveolar septae

[e]Terminal bronchioles contain luminal degenerate and necrotic cellular debris, or are lined by individual degenerate or necrotic epithelial cells and/or necrotic cell debris

Table 5

In vitro antiviral activity of various compounds in vitro against SARS-CoV Urbani and a mouse-adapted strain of SARS-CoV.

Virus Strain	Compound	Inoculum[a]	Visual Assay			Neutral Red Assay			Virus Yield Reduction	
			EC_{50}[b] µg/mL	IC_{50}[c] µg/mL	SI	EC_{50} µg/mL	IC_{50} µg/mL	SI	EC_{90}[d] µg/mL	SI[e]
v2163	Ribavirin	$10^{2.2}$	66 ± 43	>1000	15	80 ± 74	200 ± 92	2.5	83 ± 63	2.4
Urbani	Ribavirin	$10^{1.9}$	63 ± 36	>1000	16	86 ± 50	99 ± 51	1.7	104 ± 84	1.4
v2163	Promazine	$10^{2.2}$	2.6 ± 1.1	6.4 ± 2.3	2.5	8.0 ± 7.2	7.3 ± 4.2	0	3.9 ± 2.2	1.9
Urbani	Promazine	$10^{1.9}$	2.1 ± 1.0	7.9 ± 3.4	3.8	3.4 ± 2.1	8.1 ± 3.0	2.4	3.1 ± 2.1	2.6
v2163	Calpain VI Inhibitor	$10^{2.2}$	14 ± 5.4	>37	2.6	17 ± 7.3	37 ± 5.1	2.1	24 ± 7.9[f]	1.5
Urbani	Calpain VI Inhibitor	$10^{1.9}$	13 ± 2.9[f]	>37	2.8	14 ± 10[f]	27 ± 4.4	1.9	15 ± 1.0[f]	1.7
v2163	Calpain IV Inhibitor	$10^{2.2}$	4.1 ± 3.5	>56	14	9.5 ± 9.2	48 ± 19	5.1	12 ± 2.6[f]	3.9
Urbani	Calpain IV Inhibitor	$10^{1.9}$	0.87 ± 0.13	>56	64	4.3 ± 4.5	52 ± 18	12	6.4 ± 2.6[f]	8.1
v2163	Infergen™	$10^{1.9}$	<0.12	>320	>2700	<0.11	>320	>2800	<0.65	>490
Urbani	Infergen™	$10^{1.6}$	<0.29	>320	>1100	<0.31	>320	>1000	<0.65	>490
v2163	Ampligen™	$10^{1.7}$	>240	>240	1.0	>240	>240	1.0	>240	1.0
Urbani	Ampligen™	$10^{1.7}$	>240	>240	1.0	>240	>240	1.0	>240	1.0
v2163	UDA	$10^{1.7}$	0.70 ± 0.22	>10	14	0.86 ± 0.39	21 ± 9.5	24	1.1 ± 19	19
Urbani	UDA	$10^{1.7}$	0.62 ± 0.26	>10	16	0.76 ± 0.22	21 ± 9.5	27	0.95 ± 0.36	22
v2163	EP128533	$10^{2.0}$	1.4 ± 1.1	>100	>71	1.6 ± 1.6	>100	>61	12 ± 9.4	>8.5
Urbani	EP128533	$10^{1.8}$	0.56 ± 0.57	>100	>180	1.3 ± 2.1	>100	>75	5.3 ± 3.7	>19

[a] Average $CCID_{50}$ virus per well from 3 replicates.

[b] 50% effective antiviral concentration.

[c] 50% cell inhibitory concentration of drug without virus.

[d] In vitro 90% effective antiviral concentration by virus yield assay.

[e] Selective index: SI = IC_{50}/EC_{50}, and virus yield SI = IC_{50}/EC_{90}.

[f] Two replicates only.

Table 6

Cytokine responses during SARS-CoV infection of lethally-infected mice compared to humans with SARS disease.

Cytokine	Lungs of lethally-infected mice	Human lungs[a] (number of studies)	Human Serum[b] (Number of studies reviewed)
IL-1α	+	ND	ND
IL-1β	0	0 (1)	0 (2) + (3)
IL-2	0	0 (1)	0 (5) + (2)
IL-3	0		
IL-4	0	0 (1)	0 (5)
IL-5	0	ND	ND
IL-6	+	+ (1)	0 (2) + (6)
IL-9	0	ND	ND
IL-10	0	0 (1)	0 (6) + (1)
IFN-γ	+	0 (1)	0 (2) + (4)
TNF-α	0	0 (1)	0 (7) + (3)
GM-CSF	0	ND	ND
MCP-1	+	+ (1)	0 (1) + (4)
MIP-1α	+	ND	ND
RANTES	+	ND	0 (4)
IP-10	+[c]	+ (2)	+ (5)

+ = cytokine elevated 0 = cytokine not elevated ND = not determined

[a] Source: Chen and Subbarao, 2007

[b] Sources: Hsueh et al., 2004; Cameron et al., 2008, Review of Chen and Subbarao, 2007, review of Zhu, 2004.

[c] Separate study currently in press.